



HAL
open science

The resonant structure of Jupiter's Trojans asteroids-II. What happens for different configurations of the planetary system.

Philippe Robutel, Julien Bodossian

► To cite this version:

Philippe Robutel, Julien Bodossian. The resonant structure of Jupiter's Trojans asteroids-II. What happens for different configurations of the planetary system.. 2008. hal-00323327v1

HAL Id: hal-00323327

<https://hal.science/hal-00323327v1>

Preprint submitted on 20 Sep 2008 (v1), last revised 12 Jun 2009 (v2)

HAL is a multi-disciplinary open access archive for the deposit and dissemination of scientific research documents, whether they are published or not. The documents may come from teaching and research institutions in France or abroad, or from public or private research centers.

L'archive ouverte pluridisciplinaire **HAL**, est destinée au dépôt et à la diffusion de documents scientifiques de niveau recherche, publiés ou non, émanant des établissements d'enseignement et de recherche français ou étrangers, des laboratoires publics ou privés.

The resonant structure of Jupiter’s Trojans asteroids-II. What happens for different configurations of the planetary system.

P. Robutel^{1*} and J. Bodossian^{1*}

¹ *Astronomie et Systèmes Dynamiques, IMCCE, CNRS UMR 8028, Observatoire de Paris 77 Av. Denfert-Rochereau 75014 Paris, France*

20th September 2008

ABSTRACT

In a previous paper, we have found that the resonance structure of the present Jupiter Trojans swarms could be split up into four different families of resonances. Here, in a first step, we generalize these families in order to describe the resonances occurring in Trojans swarms embedded in a generic planetary system. The location of these families changing under a modification of the fundamental frequencies of the planets, we show how the resonant structure would evolve during a planetary migration. We present a general method, based on the knowledge of the fundamental frequencies of the planets and on those that can be reached by the Trojans, which makes possible the prediction and the localization of the main events arising in the swarms during migration. In particular, we show how the size and stability of the Trojans swarms are affected by the modification of the frequencies of the planets. Finally, we use this method to study the global dynamics of the Jovian Trojans swarms when Saturn migrates outward. Besides the two resonances found by Morbidelli et al. (2005) which could have led to the capture of the current population just after the crossing of the 2:1 orbital resonance, we also point out several sequences of chaotic events having been able to influence the Trojan population.

Key words: celestial mechanics – minor planets, asteroids – Solar system: general.

1 INTRODUCTION

The discovery of Achilles by Wolf in 1907, and of four other Jovian Trojans the next year, gives a new impulse to the study of the triangular configurations of the three-body problem which existence was proved by Lagrange in 1772. An important problem was to establish the existence of a stable area surrounding the triangular equilibrium points L_4 and L_5 associated to the Sun and Jupiter. From a mathematical point of view, the application of the K.A.M. theory to the circular restricted three-body problem, gives for its planar restriction, a result of confinement between two invariant torii, ensuring the stability of the neighborhood of L_4 and L_5 for an infinite time (Leontovitch 1962; Deprit & Deprit-Bartholome 1967; Markeev 1972; Meyer & Schmidt 1998). In the case of the spatial restricted three-body problem, where K.A.M. theory does not ensure infinite time stability anymore, Benettin et al. (1998) applied an extension of the Nekhoroshev theorem (1977) to quasi-convex Hamiltonian in order to prove exponentially long-time stability.

But these two complementary theories do not give any information about the size of the stable region surrounding the triangular equilibrium points. In order to get estimates of this width, several authors developed Nekhoroshev-like estimates based on normalization up to an optimal order (Giorgilli et al. 1989; Celletti & Giorgilli 1991; Giorgilli & Skokos 1997; Skokos & Dokoumetzidis 2001). More recent results, based on improvement of these methods, can be found in (Gabern et al. 2005; Efthymiopoulos & Sándor 2005; Lhotka et al. 2008). Another very interesting result was published by Rabe (1967). In this work, based on the change of stability of the family of long-period Lyapunov orbits emanating from L_4 , the author gives an approximation of the limit eccentricity of stable tadpole orbits with respect to their amplitude of libration.

Excepted Gabern and Jorba who applied the same methods as in (Giorgilli et al. 1989) to the bicircular, tricircular and biannular coherent problems (Gabern 2003; Gabern & Jorba 2004), all the above mentioned works were developed in the circular restricted three-bodies problem (RTBP) framework, planar or spatial, which is not a very realistic model for the purpose of studying the long-term

* E-mails: robutel@imcce.fr (PR); bodossian@imcce.fr (JB)

dynamics of the Jovian Trojans. To overcome this problem, several authors have performed full numerical integrations. In 1993, Holman & Wisdom, integrating test-particles during 20 Myr, obtained the first global stability result concerning the Trojans of our giant planets. Four years later, Levison et al. (1997) described the long-time erosion of the Jovian Trojans swarms without identifying its mechanism. A few years later, Michtchenko et al. (2001), Nesvorný & Dones (2002) and Marzari et al. (2003), shown the existence of two sets of unstable structures lying inside the Jovian Trojans swarms which could be related to the long-time erosion. The authors suggested that one of these sets was connected to the great inequality (between Jupiter and Saturn) while the second one may have been generated by the commensurability between the libration frequency of the co-orbital resonance and the frequency $n_{Jup} - 2n_{Sat}$. In 2005, Robutel et al. identified these singularities and exhibited their underlying resonances, this leading to the decomposition of the "resonance structure" in four families of resonances. In (Robutel & Gabern 2006), hereafter called Paper I, a new description of this resonant structure was given, and the link between these resonances and the long-term stability (or instability) of Jovian Trojan was established.

The structures described in Paper I, generated by commensurability between the proper frequencies of the Trojans and the fundamental frequencies of the planetary system, are particularly dependent on the planetary configurations. Therefore, a small modification of the geometry of the system is able to modify the Trojans swarms's resonant structure, changing dramatically the global dynamics, and the consequently stability, of the co-orbital region. The planetary migration in a planetesimal disc (see Gomes et al. (2004) and references therein) provides a natural mechanism of evolution of planetary systems. According to Morbidelli et al. (2005), the Jovian co-orbital population is not primordial, but has rather been captured during chaotic events during the planetary migration. The so-called Nice model (Tsiganis et al. 2005) predicts that during the migration (inward for Jupiter, and outward for Saturn, Uranus and Neptune), the couple Jupiter-Saturn has crossed the 2:1 orbital resonance. Morbidelli et al. (2005) suggest that the Trojans have been captured in co-orbital motion just after the crossing of this resonance, when the dynamics of the Trojan region was completely chaotic. The authors show that this global chaos arises when the libration frequency of the Trojans is close to the combinations $3(n_{Jup} - 2n_{Sat})$ or $2(n_{Jup} - 2n_{Sat})$. This result was recently confirmed by Marzari & Scholl (2007), showing that these resonances are the main generators of the depletion (and probably the capture) of the Trojan population.

The results reported in Paper I are directly related to the phenomenon described in Morbidelli et al. (2005) and Marzari & Scholl (2007). More precisely, the resonances involved in this process are members of one of the four families of resonances presented in Paper I. Consequently, this previous paper contains the necessary material to derive tools making possible the study of the evolution of the Trojans resonant structure induced by changes of the geometry of the considered planetary system. Indeed, our goal is not to give an accurate and realistic description of the behavior of the Trojans swarms during a migration process, but rather to know what are the planetary configurations for which the

Trojans swarms become globally chaotic. Moreover, we want to develop a model of prediction applicable to a large class of problems, in order to be not restricted to the study of the Jovian Trojans. This method is based on three different points. The first one rests on the understanding of the Trojans resonant structure, and its decomposition. It will be shown in section 2 that, for a generic Trojans swarm, almost all resonances driving its global dynamics are members of four different families which generalize the one described in Paper I. All the resonances of these families involve both Trojan's fundamental frequencies and the basic planetary frequencies. These families establish the link between the behavior of the Trojans swarm and the geometry of its planetary system. The two others ingredients on which the method is based are respectively the fundamental planetary frequencies and the frequency domain to which belong the main frequencies of the whole Trojans swarm. In section 3 our method is applied to the study of the Jovian Trojans perturbed by Saturn, model used in Paper I but also in (Morbidelli et al. 2005; Marzari & Scholl 2007). This application reveals the dynamical richness of the Trojans swarms under the action of numerous resonances of different nature, resonance web which cannot be fully understood without knowing the fundamental frequencies of the considered dynamical system.

2 THE RESONANCE STRUCTURE OF A GENERAL TROJANS SWARM

2.1 General setting

Let us consider a general case: the planet harboring Trojans swarms is the p^{th} planet of a given planetary system composed of N planets orbiting a central star. We denote by m_j , respectively a_j , the masses and the semi-major axes of the planets, and m_0 the mass of the star. The small mass parameter μ is defined by the expression $\mu = \max(m_1/M, \dots, m_N/M)$, where M is the total mass of the system. A linear combination of secular frequencies will be denoted: $\mathbf{k}_g \cdot \boldsymbol{\sigma}_g + \mathbf{l}_s \cdot \boldsymbol{\sigma}_s$ where \mathbf{k}_g and \mathbf{l}_s are elements of \mathbb{Z}^N . If we assume that the planetary system is stable enough to be considered as quasiperiodic for a given time length (see paper I), its fundamental frequencies are denoted: (n_1, \dots, n_N) , $\boldsymbol{\sigma}_g = (g_1, \dots, g_N)$ and $\boldsymbol{\sigma}_s = (s_1, \dots, s_N)$ ¹, where the n_j denote the proper mean motions which are of order 0 with respect to the planetary masses. The vectors $\boldsymbol{\sigma}_g$ and $\boldsymbol{\sigma}_s$ correspond to the secular frequencies of the planetary system (respectively associated to the precession of the perihelia and to the precession of the ascending nodes) which are of order μ .

2.2 Restricted three-body problem

In a first step, we retain only the gravitational interaction of the p 'th planet (and of the star) on the Trojans. We are thus brought back to the restricted three-body problem (R.T.B.P). This model gives, at least for the outer planets of the solar system, results which are quite realistic (it is not the case for our inner planets, see section

¹ Owing to invariance by rotation, one of the s_j is zero.

2.3). In this model, the triangular equilibrium points L_4 or L_5 are well defined, even for an elliptic motion of the planet (paper I). When the motion of the secondary is circular, these fixed points are elliptic (linearly stable) while the inequality $27m_p m_0 < (m_p + m_0)^2$ is satisfied (Gascheau 1843). This ensures the linear stability of the equilateral equilibria as soon as μ belongs to the interval $[0, \mu_0]$, with $\mu_0 = (1 - \sqrt{23/27})/2 \approx 0.0385$. For eccentric motions of the secondary, the (linear) stability criterion depends on its eccentricity, and stability exists for values of μ greater than μ_0 (see (Danby 1964; Roberts 2002) for numerical estimates and (Meyer & Schmidt 2005) for analytical ones). When the equilibrium is linearly stable, the eigenfrequencies (modulus of the eigenvalues) $\nu_{L_{4,5}}$, $g_{L_{4,5}}$ and $s_{L_{4,5}}$, respectively the fundamental frequency associated to libration, to the perihelion of the Trojan and to its ascending node, are given by:

$$\begin{aligned} \nu_{L_{4,5}} &= \sqrt{(27/4)\varepsilon n_p} + o(\sqrt{\varepsilon}) = O(\sqrt{\mu}), \\ g_{L_{4,5}} &= (27/8)\varepsilon n_p + o(\varepsilon) = O(\mu) \\ s_{L_{4,5}} &= 0 \quad \text{with } \varepsilon = \frac{m_p}{m_0 + m_p} = O(\mu). \end{aligned} \quad (1)$$

General theory gives the values of the frequencies not only at the Lagrangian points, but in the tadpole region and also for horseshoes orbits (Garfinkel 1976; Morais 2001). According to these theories, the frequency magnitude remains the same in the whole phase space, except for s which reach the order $O(\mu)$ but remains always lower than g (absolute value). Owing to these three different time scales, significant resonances between these frequencies are very unlikely (at least asymptotically). In the present solar system, these resonances are negligible as long as μ is lower than 10^{-3} (close to Jupiter mass). Several regions of the Jupiter's Trojans swarms are deeply affected by secondary resonances involving commensurability between the libration frequency and Jupiter's proper mean motion. In Paper I, these resonances, elements of *Family I*, are defined by:

$$i\nu + jn_p + kg = 0, \quad (i, j, k) \in \mathbb{Z}^3. \quad (2)$$

For Jupiter's Trojans swarms, among this family, the influence of the resonances satisfying $j = 1$ and $i \in \{12, 13, 14\}$ is dominant for moderate to high libration amplitude. In the present paper, the three resonances can be seen in Fig. 5 (see section 2.3). Although the dynamical implication of these resonances is weaker in the circular RTBP than in the elliptic one, *Family I* is well known in the first model. Indeed, the existence of denominators associated to the resonances $(i, j) \in \{(11 : -1), (12 : -1), (13 : -1), (14 : -1)\}$ during the Birkhoff normalization process is already mentioned in (Deprit et al. 1967). But these terms do not generate any difficulty up to degree 15. More over, those resonances are identified in (Giorgilli et al. 1989) as the factor of divergence of the normal forms in the spatial circular RTBP. Érdi et al. (2007) study in details these secondary resonances in the elliptic RTBP. and their dependence on the mass and eccentricity of the secondary.

2.3 Restricted (N+2)-body problem

The first difficulty comes from the fact that, in the restricted (N+2)-body problem, since N is greater or equal to 2, the triangular equilibrium points do not exist. These points are at most replaced by elliptic quasiperiodic trajectories (see (Jorba & Simó 1996; Jorba 2000; Gabern 2003)). But numerical experiments show that, if the additional planetary perturbations are not too large, a stable region remains in the neighborhood of the equilateral points. Like in the RTBP, these equilateral points, which are always properly defined, are usually called L_4 and L_5 .

Once this point clarified, let us study the influence of planetary perturbations on the Trojans associated to the p^{th} planet. These dynamical effects on the Trojans swarms can be mainly split in two classes: the direct influences, due to the gravitational attraction of the planets on the Trojans; and the indirect effects, coming from the fact that the p^{th} planet evolves no more on a Keplerian trajectory². Although this difference between direct and indirect perturbation is quite arbitrary, we will see later that in some cases these two phenomena are mixed together, it has the advantage to simplify the discussion. In terms of frequencies, the main effect of the direct influences is to modify the proper frequencies (ν, g, s) of the Trojans. Assuming that the motion of the additional planets is circular (we consider here the N -circular problem), according to the Laplace-Lagrange theory, the secular linear contribution of the j^{th} planet to the proper precession frequency g can be roughly approximated at L_4 (or L_5) by the expression:

$$g_{L_{4,5}}^{(j)} = \frac{1}{4} n_p \mu_j \alpha_j b_{3/2}^{(1)}(\alpha_j), \quad \text{if } \alpha_j = \frac{a_j}{a_p} < 1. \quad (3)$$

$$g_{L_{4,5}}^{(j)} = \frac{1}{4} n_p \mu_j \alpha_j^2 b_{3/2}^{(1)}(\alpha_j), \quad \text{if } \alpha_j = \frac{a_p}{a_j} < 1. \quad (4)$$

where $b_{3/2}^{(1)}$ is a Laplace coefficient and $\mu_j = m_j/m_0$ (see for example (Murray & Dermott 1999)). Then, the secular frequencies at the triangular equilibrium points are given by:

$$g_{L_{4,5}}^{(Tot)} = g_{L_{4,5}}^{(R.T.B)} + \sum_{j \neq p} g_{L_{4,5}}^{(j)} \quad (5)$$

$$s_{L_{4,5}}^{(Tot)} = s_{L_{4,5}}^{(R.T.B)} - \sum_{j \neq p} g_{L_{4,5}}^{(j)} \quad (6)$$

where $g_{L_{4,5}}^{(R.T.B)} = (27/8)\varepsilon n_p$ and $s_{L_{4,5}}^{(R.T.B)} = 0$, see formulas (1). The frequencies $g_{L_{4,5}}^{(Tot)}$ and $s_{L_{4,5}}^{(Tot)}$ as well as $g_{L_{4,5}}^{(R.T.B)}$ and the planetary contribution $g_{L_{4,5}}^{(plan)} = \sum_{j \neq p} g_{L_{4,5}}^{(j)}$ are gathered in Table (1), for every planet of the solar system. Although the results of Table (1) are valid only at the triangular points and for circular and coplanar planetary orbits, they are enough to deduce striking conclusions. As we can see by comparison of the second and third column, the planetary contribution $g_{L_{4,5}}^{(plan)}$ is not always a perturbation, but, at least for Mercury, Mars and Uranus, the main contribution to the precession frequencies. It is only for Saturn and mainly for Jupiter that the direct planetary

² In order to clarify the following discussion, we consider in this section that the motions are quasiperiodic, which is not necessary

perturbations impose only small perturbations to their Trojans. Consequently, except for Jupiter, the planetary direct gravitational attraction drastically modified the dynamics predicted by the RTBP. This phenomenon has been emphasized by Tabachnik & Evans (2000) in the case of Mercury’s Trojans. Indeed, in the full solar system model, the authors found that the most stable zones (100 Mys stability) did not contain the Lagrange points. Another striking point is that, in an outer solar system simulation, the region of smallest amplitude of libration of Uranian and Neptunian Trojans is shifted by more than $0.1AU$ from its predicted location in the RTBP (Nesvorný & Dones 2002).

The indirect perturbations act on a more subtle way than the direct ones: the introduction of forcing frequencies enables resonances between the Trojan’s frequencies and these additional frequencies. Obviously, the secondary resonances with the orbital frequency n_p is directly affected by the additional secular frequencies. These forcing frequencies increase the number of possible resonant harmonics, imposing a generalization of *Family I* by:

$$i\nu + jn_p = -(kg + ls + \mathbf{k}_g \cdot \boldsymbol{\sigma}_g + \mathbf{l}_s \cdot \boldsymbol{\sigma}_s). \quad (7)$$

with $i \neq 0$, $j \neq 0$ and $j+k+l+\mathbf{k}_g \cdot \mathbf{1} + \mathbf{l}_s \cdot \mathbf{1} = 0$. In these expressions the dot denotes the Euclidian scalar product and $\mathbf{1} = (1, \dots, 1)$. The enrichment of this family may generate large chaotic regions generated by the overlap of those resonances. Another expected consequence is the introduction of secular resonances. As is shown by the two last columns of Table 1, except for the frequency g of Jupiter and Saturn Trojans, in the solar system, the secular frequencies at L_4 are very close to the fundamental frequencies of the perihelia and of the nodes of the planets (Laskar 1990; Laskar et al. 2004). Indeed, the resonance $s = s_2$ which limits the long-term stability region of low inclination Jovian Trojans was first mentioned by Yoder (1979), other secular resonances involving s are discussed in (Milani 1993, 1994). The role of secular resonances on the motion of the Trojans of Terrestrial planets was investigated by Brassier & Lehto (2002). More accurate studies were dedicated to secular resonances and the dynamics of Venus Trojans (Michel 1997; Scholl et al. 2005b) and Mars Trojans (Scholl et al. 2005a). Like in Paper I, the family containing secular resonances is denoted *Family III* and defined by:

$$kg + ls + \mathbf{k}_g \boldsymbol{\sigma}_g + \mathbf{l}_s \boldsymbol{\sigma}_s = 0. \quad (8)$$

Contrarily to Paper I, where k is always equal to zero, the opportunity that $k \neq 0$ in Jupiter’s Trojans swarms is discussed in sections 3.1.2 and 3.3.

The conjunction of both direct perturbations and secular resonances prevents tellurian planets, Mars excepted (Scholl et al. 2005a), from having long-live Trojans. For this reason, the Trojans of the three first planets of the solar system are generally transient objects, which spend only a few hundreds of thousand years in the co-orbital region (Morais & Morbidelli 2002, 2006).

Until now, only secular forcing frequencies have been taken into consideration, but combinations of planetary mean-motions play also a major role in some specific configurations of the planetary system. If we consider an $\beta : \alpha$ MMR between the p^{th} planet and another one ³, let say the

³ Three-bodies and more MMR are not taken into account here.

Table 1. Linear secular frequencies evaluated at the triangular points of the planets of the solar system expressed in arcsec yr^{-1} . In the first column is given the name of the planets. The second one gives the precession frequency of the perihelion derived from the circular RTBP: formula (1), while the third one gathered the contribution of the planets to this frequency (formula 6). Finally, the precession frequencies g and s at L_4 or L_5 are given in fourth and fifth columns.

	$g_{L_{4,5}}^{(R.T.B.)}$	$g_{L_{4,5}}^{(plan)}$	$g_{L_{4,5}}^{(Tot)}$	$s_{L_{4,5}}^{(Tot)}$
Me	3.0	5.5	8.5	-5.5
V	17.3	12.2	29.5	-12.2
E	13.3	12.9	26.2	-12.9
Ma	0.7	17.8	18.6	-17.8
J	352.3	7.4	359.8	-7.4
S	42.3	18.3	60.6	-18.3
U	2.3	2.7	5.0	-2.7
N	1.4	0.7	2.0	-0.7

q^{th} , which critical angle is

$$\theta = \alpha\lambda_p - \beta\lambda_q + \dots, \quad (9)$$

where the dots represent a linear combination of longitudes of the nodes and of the perihelia such that d’Alembert rules are satisfied, the modulus of the quantity $\nu_{\alpha,\beta} = \alpha n_p - \beta n_q$ will depend on the closeness of the planetary system to the resonance. The closest to the resonance the system will be, the smallest $|\nu_{\alpha,\beta}|$ will be (see Fig. 1). Hence, far from the MMR, $\nu_{\alpha,\beta} = O(1)$ (same order of the one of the planetary mean motions). If the two planets are closer to the resonance, the frequency $\nu_{\alpha,\beta}$ becomes of order $O(\sqrt{\varepsilon})$ which is of the same order than ν . This makes possible commensurabilities of these frequencies leading to the family of resonances called *Family II*, defined by:

$$i\nu - j\nu_{\alpha,\beta} = -(kg + ls + \mathbf{k}_g \cdot \boldsymbol{\sigma}_g + \mathbf{l}_s \cdot \boldsymbol{\sigma}_s) \quad (10)$$

with $j(\beta - \alpha) + k + l + \mathbf{k}_g \cdot \mathbf{1} + \mathbf{l}_s \cdot \mathbf{1} = 0$. This generalizes *Family II* defined in Paper I. Very close to the MMR, $\nu_{\alpha,\beta}$ reaches the order $O(\varepsilon)$ and commensurability between $\nu_{\alpha,\beta}$ and g can arise. These resonances are described by *Family IV* satisfying:

$$j\nu_{\alpha,\beta} + kg = -(ls + \mathbf{k}_g \cdot \boldsymbol{\sigma}_g + \mathbf{l}_s \cdot \boldsymbol{\sigma}_s) \quad (11)$$

with $j(\alpha - \beta) + k + l + \mathbf{k}_g \cdot \mathbf{1} + \mathbf{l}_s \cdot \mathbf{1} = 0$. This generalizes the family *Family IV* defined in Paper I.

3 AN APPLICATION TO JUPITER’S TROJANS

3.1 One parameter model

3.1.1 Model and method of analysis

In this section, the evolution of the resonant structure in the Trojans swarms mentioned in section 2.3 will be illustrated using a concrete planetary system. To this purpose, the methods described in Paper I will be followed. We consider the planetary system made of the Sun, Jupiter and Saturn. In order to be consistent with the previous section 3.1.1, the index 1 is associated to Jupiter and 2 to Saturn. In Paper I, the system, in its present configuration, is close to the 5:2 MMR, consequently, resonances of *Family IV* should

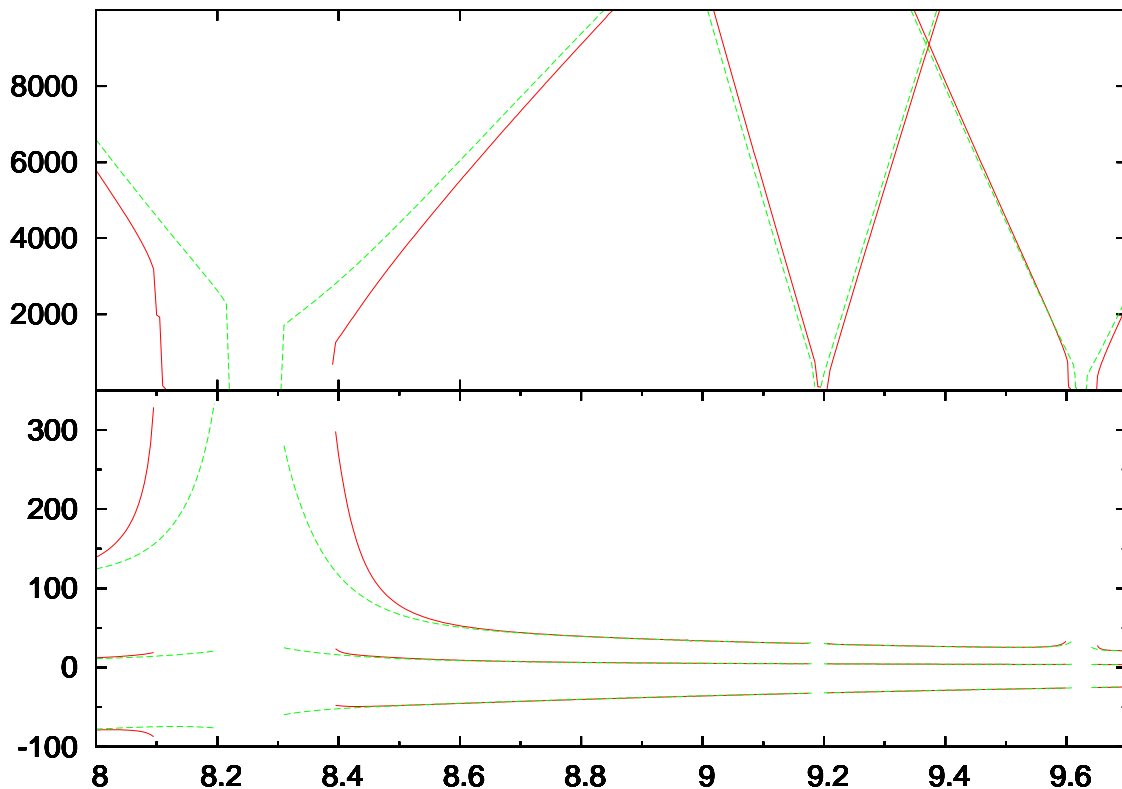


Figure 1. Fundamental frequencies of the planetary system versus a_2 . Top: combinations of frequencies $|\nu_{1,2}|$, $|\nu_{3,7}|$ and $|\nu_{2,5}|$ which are associated to the resonances of *Family II*. Bottom: secular frequencies g_1 , g_2 and s_2 . The empty intervals correspond to the MMR 2:1, 7:3 and 5:2 where the secular frequencies are singular. The frequencies associated to the "elliptic" section of the phase space ($M_2 = 340.04^\circ$) are plotted in red, while the "hyperbolic" section ($M_2 = 24.14^\circ$) is in green. See the text for more details

be present in the Trojans phase space. Indeed, several resonances of this family (for $j = 1$ and $k = 4$ in formula (11)), have been clearly identified in Paper I. We have shown in this paper, that these resonances are associated to the long-term erosion of the Trojans swarm.

Despite the long distance between the theoretical location of the 2:1 and the present couple of giant planets (more than $1.2AU$) resonances members of *Family II* associated to $\nu_{2,1}$ have been also clearly identified. Owing this distance, the combinations between ν and $\nu_{1,2}$ are of high order: $i = 5$ and $j = -2$ in formula (10). Obviously, secondary resonances of *Family I* and secular resonances numbers of *Family III* play a major role in the present Jupiter's Trojans swarms (Paper I). But, as these families are only weakly affected by migration (section 3.1.2), except very close to MMR (sections 3.3), we will not really pay attention to these resonances.

In order to appreciate the modifications of the resonant structure of Jupiter's Trojans due to different relative positions (and distances) between the two planets, we consider a sequence of independent planetary initial conditions. The fundamental frequencies of the planetary system depending mainly on the semi-major axes of the planets, or more precisely on its ratio, we have decided to change only one parameter: the semi-major axis of Saturn a_2 . Hence, we are left with a one-parameter model. More concretely, for every values of the parameter a_2 , we integrate the Sun, Jupiter,

Saturn and a set of fictitious Jupiter's Trojans (considered as test-particles). Except for the initial Saturn's semi-major axis, which is chosen in-between 8 and 9.7 AU, the initial conditions of Jupiter and Saturn are the ones given by DE405 at the Julian date 245 2200.5 (2001 October 10). As regards the Trojans swarms, the initial elements of its members are independent of the parameter. In each run, 200 initial semi-major axis and 40 eccentricities are equally spaced in the domain $\mathcal{A} = [5.2035, 5.4030] \times [0.05, 0.30]$ (8000 test-particles), while the other elements are fixed to the following values: $\sigma = \lambda - \lambda_1 = \pi/3$, $\sigma_g = \varpi - \varpi_1 = \pi/3$, $\Omega = \Omega_1$ and $I = I_1 + I^*$. Because the resonant structure depends on the initial inclination (Paper I), I^* is fixed to three different values: 2° , 20° and 30° . In this paper, this set of initial conditions is denoted \mathcal{D}_{I^*} .

The numerical simulations are performed by the symplectic integrator *SABA4* (Laskar & Robutel 2001) with an integration step of 1/2 year. Trojans and planets are integrated on two consecutive time-span of $5Myr$. For particles surviving the integration (bodies which are not ejected from the co-orbital region before the end of the integration) fundamental frequencies are computed for each of these two time-intervals by the mean of frequency analysis method developed by Laskar (1990). If we denote by \mathcal{F} the map which associates to each Trojan of \mathcal{D}_{I^*} its fundamental frequencies (ν, g, s) (see Laskar 1999 and Paper I), the domain of the frequency space reached by the Trojans is: $\Theta_{I^*} = \mathcal{F}(\mathcal{D}_{I^*})$.

Consequently, three complementary informations are derived from the study of \mathcal{D}_{I^*} . The most straightforward information is given by the escape rate: number of Trojans escaping the co-orbital region before the end of the integration (10 My), divided by the initial number of Trojans inside \mathcal{D}_{I^*} (see Fig.8). Owing a lost of accuracy of our integrator during close encounter with Jupiter, the depletion of \mathcal{D}_{I^*} is probably over estimated, but in any case, this ejection rate is always correlated to the global instability of the considered region (see section 3.3). The other informations regard the fundamental frequencies. As a detailed discussion of the application of Frequency Map Analysis to the Trojans can be found in Paper I, let us just sum up two applications of this method. Firstly, the comparison of the set of frequencies computed on the two steps of $5Myr$ makes it possible to derive the diffusion rate of every Trojan (index related to its stability). From this index, a dynamical map of the domain \mathcal{D}_{I^*} is derived. Secondly, the study of the frequency domain Θ_{I^*} enable us to understand how the chaotic regions are generated, by the determination of the underlying resonances. Fig.5 and 6 provide illustrations of the application of these complementary techniques.

Once known the fundamental planetary frequencies along the segment $a_2 \in [8, 9.7]$ (section 3.1.2), it is straightforward to predict whether the families of resonances are inside the Trojans phase space or not. Obviously, in order to make these predictions, the bounds of the frequency domain Θ_{I^*} have to be known. To this aim, we assume that these bounds do not depend on the value of a_2 , which is a very good approximation in the case of Jupiter's Trojans. As it was established in Paper I, we assume in the following sections that:

$$\begin{aligned} \Theta_2 &\subset [7700, 9150] \times [310, 445] \times [-45, -7.5] \\ \Theta_{20} &\subset [7400, 8660] \times [285, 350] \times [-40, -3.5] \\ \Theta_{30} &\subset [7000, 8138] \times [251, 280] \times [-30, +0.6] \end{aligned} \quad (12)$$

where the three intervals are respectively the projections of Θ_{I^*} on the 1-dimensional space of ν , g and s denoted $\pi_\nu(\Theta_{I^*})$, $\pi_g(\Theta_{I^*})$ and $\pi_s(\Theta_{I^*})$. It is important to mention that the lower bounds of ν and s are here arbitrary. For example, at 2° of initial inclination, Trojans whose libration frequency is lower than about 7800 arcsec yr $^{-1}$ have trajectories relatively far to be quasi-periodic, making less significant the use of fundamental frequencies (details can be found in Paper I). The same remark holds when s is lower than the bounds indicated in (12). These bounds may also be compared to those obtained by analytical fits of (ν, g, s) (Milani 1994; Marzari et al. 2003), which gives quite similar results up to 30° of initial inclination.

3.1.2 Behavior of the planetary frequencies

From now on, Jupiter and Saturn semi major axes and proper mean motions are denoted (a_1, a_2) and (n_1, n_2) . In the same way, the secular frequencies are $\sigma_g = (g_1, g_2)$ and $\sigma_s = (s_1, s_2)$. These frequencies playing a basic role in this study, it is therefore essential to know their variations with respect to our parameter a_2 . Jupiter's proper mean motion n_1 is practically not affected by the variations of a_2 . As a result, the location of the resonances of *Family I* is almost independent of the value of a_2 . Only small shifts are observable due to the variation of the secular frequencies involved

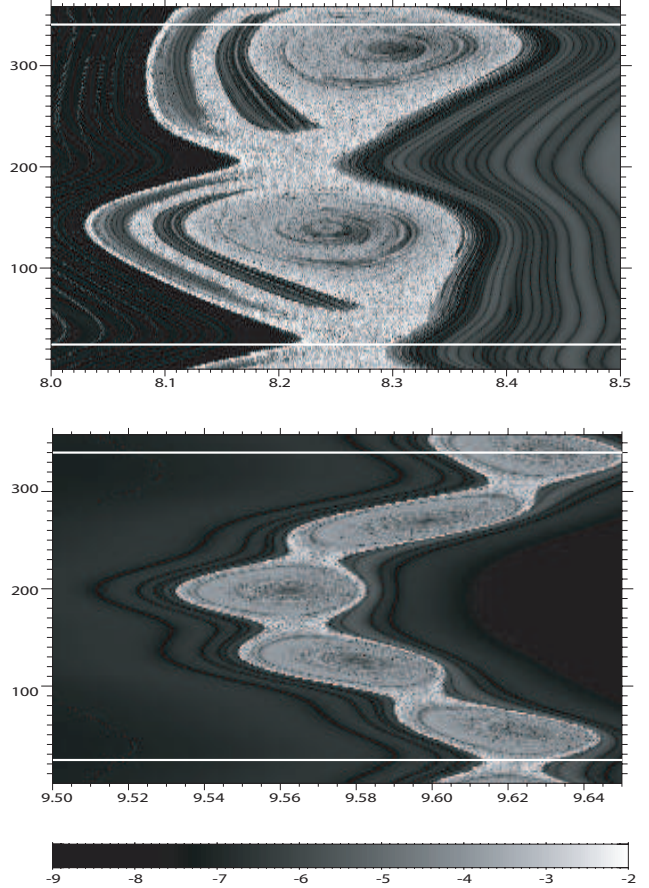


Figure 2. Section of the phase space of the planetary system by the plane of initial conditions (a_2, M_2) . Neighborhood of the mean motion resonance 2:1 (top) and 5:2 (bottom). The small bottom strip displays the grey code associated to the diffusion index: the darker is the grey, the more regular are the trajectories. The two horizontal white lines corresponds respectively to the "elliptic segment" for $M_2 = 340.04^\circ$ and to the "hyperbolic segment" for $M_2 = 24.14^\circ$

in formula (7). On the contrary, n_2 being affected by the variation of the parameter, the mean motion combinations associated to orbital resonances (here $\nu_{1,2}$, $\nu_{3,7}$ and $\nu_{2,5}$) vary drastically⁴, enable the resonances of *Family II* to go through the whole Trojans swarm. These frequencies are plotted in red in Fig. 1 (top), which clearly illustrates the discussion of section 2.3. Before going further, we have to mention that the quantity $\nu_{\alpha,\beta}$, as long as $\beta > 0$, is an increasing function of a_2 . Even if it is more convenient to plot $|\nu_{\alpha,\beta}|$ rather than its signed value, we have to keep in mind that this frequency is positive before an orbital resonance (i.e. when a_2 is smaller than the Saturn's semi-major axis required to be in MMR with Jupiter) and positive after. When a_2 evolves toward a MMR, the corresponding combination $|\nu_{\alpha,\beta}|$ decrease toward zero. First, this frequency

⁴ Only these three resonances are taken into account in our study. Other higher order MMR like the 9:4, 11:5 and 12:5 are also present in the domain of study, but their influence on the Trojans remains too small to be considered in the present study

reach values close to $8000 \text{ arcsec yr}^{-1}$ giving rise to the resonances $\nu \approx \nu_{\alpha,\beta}$ of the second family, then $\nu \approx 2\nu_{\alpha,\beta}$ and so on, until $\nu_{\alpha,\beta}$ is of order of a few g where *Family IV* takes place. When the planetary system crosses the resonance, the frequency $\nu_{\alpha,\beta}$, which is equal or at least very close to zero, suffers from chaotic variations due to the dynamical structures encountered inside the MMR (see Fig. 2). For the sake of clarity, the behavior of the frequencies inside orbital resonances is not reproduced in Fig. 1. This leads to gaps in the curves representing the frequencies. On both sides of these gaps, the singularities generated by the stable and unstable manifold of the resonance imposes the frequencies to go to infinity.

The bottom frame of Fig. 1 displays the values of the secular frequencies (red curves) with respect to a_2 . The negative frequency is s_2 , while the two positive frequencies are g_1 and g_2 knowing that $g_1 < g_2$. The general trend of the absolute value of the secular frequencies is to decrease when a_2 increase. This is merely due to the fact that the perturbations between the two planets decrease with respect to their mutual distance. But, as for the combinations of mean motions, singularities appear when the "separatrix" of the MMRs are reached. The rise of the secular frequencies is particularly striking on both sides of the 2:1 MMR. Here, as it can be also seen in a small neighborhood of the 7:3 and the 5:2, g_2 is much more affected than the two other secular frequencies. More precisely, these three frequencies have to go to infinity, but the growth of the slope begins farther from the "separatrix" for g_2 than for g_1 and s_2 (see Fig. 1). As a result, we would expect to detect the influence of the secular resonances of *Family III* like the $g = (k+1)g_2 - kg_1$ for at least small values of $|k|$. But, as large values of g_1 and g_2 are necessary to reach these resonances, this phenomena occurs only very close to the 2:1 MMR. As it will be shown in section 3.3, instability is so strong in this region that secular resonances cannot be isolated and clearly identified.

The approach of a MMR is characterized by a sharp and sudden variation of the planetary fundamental frequencies corresponding to the singularity associated to the separatrix. But the location of these asymptotes depend on the initial angles of the planets (M, ω, Ω). It is therefore interesting to know the geometry of the orbital resonances in the phase space. Fig. 2 shows dynamical maps of the regions surrounding the orbital resonance 2:1 (top) and 5:2 (bottom), corresponding to the section of the phase space with the plane of coordinates (a_2, M_2) , M_2 being the mean anomaly of Saturn. The grey code indicates the diffusion rate of Saturn's proper mean motion computed on two consecutive time intervals (section 3.1.1). From these two determinations, denoted respectively $n_2^{(1)}$ and $n_2^{(2)}$, a diffusion index is derived by the expression: $\log_{10} |(n_2^{(1)} - n_2^{(2)})/n_2^{(1)}|$. The structures of high diffusion rate (light grey for diffusion rate greater than -3) are associated to the inner part of the resonance (libration island). Fig. 2 shows the characteristic shape of the resonant chains composed of two islands for the 2:1 and five for the 5:2 (see Robutel & Laskar (2001) for details). These large islands corresponding to globally stable regions (elliptic regions in the pendulum model) are separated by narrow unstable structures like the hyperbolic fixed points in the simple case of the pendulum. Even if the dynamics of this problem is a bit out of the scope of

this paper, two points are interesting to notice. First of all, the dynamics inside the resonant islands seems to be very rich. Indeed, very sharp structures indicated by different diffusion rates are clearly visible, they are probably related to secondary or secular resonances. The second point lies in the fact that, particularly for the 5:2, the island chain is strongly distorted, making uneasy to define a resonance width. The segment containing the initial conditions used for our simulation is represented in Fig. 2. Along this segment, the initial values of M_2 are always equal to $M_2 = 340.04^\circ$. This line of initial conditions crosses the first lobe of the 2:1 orbital resonance practically along its widest section, and passes near the libration center. For this reason, we call it "elliptic segment". According to Morbidelli et al. (2005), during planetary migration, the MMRs and particularly the 2:1 is "jumped" by the planetary system. More precisely, if the migration is slow enough to satisfy the adiabatic invariance hypothesis, the system has to cross the resonance through its hyperbolic fixed point (this make sense for one degree of freedom systems) without reaching any libration zone (the same phenomenon is observed in Marzari & Scholl 2007). In order to compare the "elliptic crossing" to the "hyperbolic" one, we consider a second set of initial conditions represented in Fig. 2 by the second horizontal white line ($M_2 = 24.14^\circ$). We also notice in Fig.2 (bottom) that this segment passes through the hyperbolic region connecting the lobes of the 5:2 resonance. Since the red curves are associated to the planetary frequencies computing along the "elliptic segment" in Fig.1, the green curves correspond to the same frequencies but derived from the "hyperbolic segment". The behavior of the frequencies along the "hyperbolic segment" is qualitatively the same along the "elliptic segment", except near the three dominant MMRs, where the singularities are shifted as predicted by Fig. 2. The consequences of this shift on the Trojans, will be studied in the end of section 3.3.

3.2 Sweeping of *Family IV*'s resonances across the Trojan region.

3.2.1 Prediction of the location of *Family IV*'s resonances

In this section we focus our attention to the close neighborhood of the orbital resonance 5:2. Indeed, we have shown in Paper I that the system is close enough to this resonance to give rise to narrow unstable regions resulting from *Family IV*. Even if these chaotic regions seems very thin, several resonances of this family are involved in the low erosion process of the Jupiter's Trojans swarms first mentioned by Levison et al. (1997). Because between the current location of the system and the 5:2 MMR the Trojans will encounter several resonances of this family, the study of this region enable us to describe and illustrate accurately the crossing of the Trojans swarms by the resonances of *Family IV*.

The resonances of *Family IV*, defined by formula (11), involve the frequencies $\nu_{2,5}$, g , and the secular frequencies of the planetary system. According to Fig.1 and formula (12), the variations of g_1, g_2, s_2 are small with respect to those of $\nu_{2,5}$. Furthermore, the secular frequencies of the planets are small compared to g , except very close to the 2:1 MMR (see latter). As a result, the location of *Family IV* depends mainly on the values of $\nu_{2,5}(a_2)$. The variation

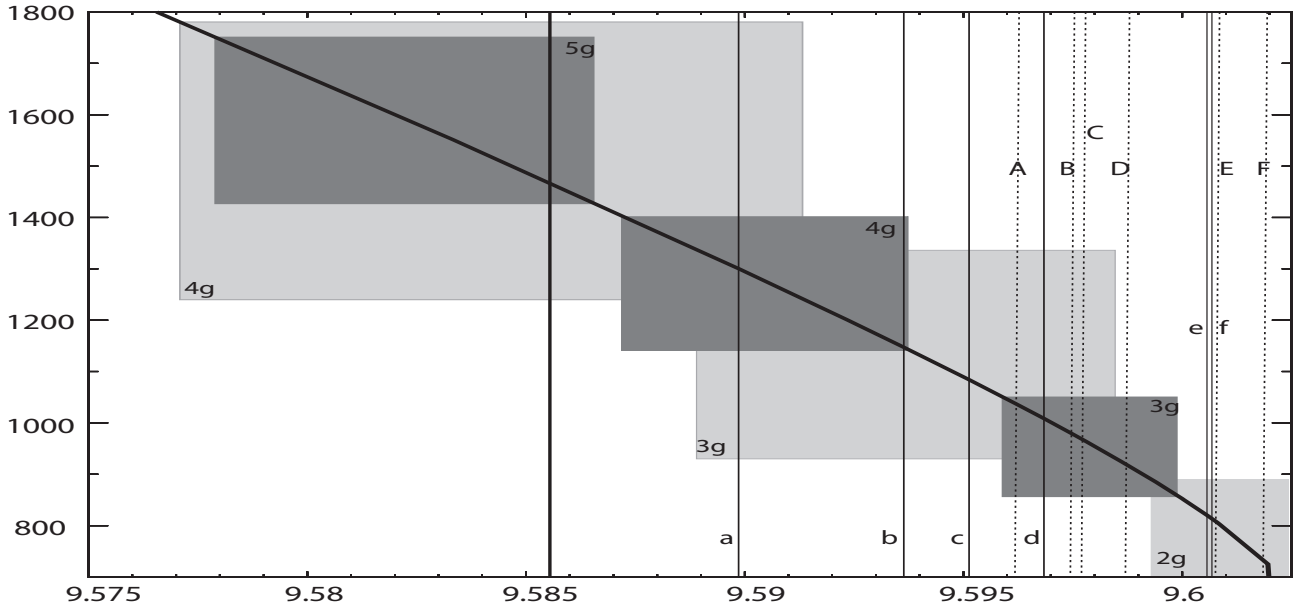


Figure 3. Crossing of the Trojans swarms by the resonances of *Family IV*. The slanted bold black curve represents the values of $-\nu_{2,5}$ (arcsec yr $^{-1}$) versus a_2 (AU). The grey rectangles indicate the values of (a_2, ν) for which a subfamily of *Family IV* is inside the swarms. The light grey is used for $I^* = 2^\circ$ and dark grey for 20° . The vertical bold line near 9.585AU corresponds to the present location of Saturn. The other lines indicate the value of a_2 used in the numerical simulations "a" to "f" ($I^* = 2^\circ$) and "A" to "F" ($I^* = 20^\circ$). See the text for details.

of this frequency with respect to a_2 is plotted in figure 3. More precisely, the bold curve of this picture represents the graph of the function $f: x \mapsto -\nu_{2,5}(x)$. The X-axis corresponds to the initial values of a_2 (in AU) while the Y-axis is associated to the frequencies (in arcsec yr $^{-1}$). This curve decreases very regularly, until a_2 reaches 9.602AU , where a sharp change of slope indicates the beginning of the 5:2 MMR (see also Fig.2, bottom-frame). It is now straightforward to predict the location of resonances belonging to *Family IV* in the Trojan phase space. Indeed, as long as the right side of (11) is negligible with respect to kg , the resonant condition is well approximated by the relation:

$$-\nu_{2,5}(a_2) \in \frac{k}{j}\pi_g(\Theta_{I^*}). \quad (13)$$

For given values of j and k , the previous formula defines a frequency interval where the resonance is reached. The bold curve in Fig. 3 being smooth and monotonic, f^{-1} maps this interval in another one of the X-axis⁵, namely: $f^{-1}(k/j\pi_g(\Theta_{I^*}))$. The cartesian product of these two intervals, the first one on the frequency axis (Y) and the second one on the a_2 axis (X), defines a "resonant rectangle" displayed in gray in Fig.3, and denoted by $R_{I^*}^k$.

For the sake of clarity, our study is limited to the resonances defined by $j = 1$ and $k > 0$ ($k < 0$ on the other side of the MMR). According to (12) and (13), the location of the resonances of *Family IV* depend on the initial inclination I^* . For this reason, we study sections of the phase

space at two initial inclinations: $I^* = 2^\circ$ and $I^* = 20^\circ$. The corresponding resonant rectangles are colored in light grey and dark grey respectively. The value of k associated to each box is indicated by the labels 5g, 4g, 3g and 2g in its bottom-left corner at 2° and its top-right corner at 20° . Fig.3 shows that, for a given k , the size of the $R_{I^*}^k$ decreases with I^* , and that for a fixed I^* , these rectangles are shifted rightwards when k decrease. This two phenomena are due to the facts that the function f is decreasing and concave, and that the width and the bounds of $\pi_g(\Theta_{I^*})$ decrease while I^* increases. One of the main consequences of these properties lies on the fact that *Family IV* enters the Trojans swarms for a value of a_2 which depends on I^* . Therefore, during a migration (slow monotonic variation of a_2 with respect to the time in the studied region), *Family IV*'s resonances will sweep through the Trojans phase space in a way depending on the inclination: $R_{2^\circ}^k$ being larger the one at $R_{20^\circ}^k$. It follows that the instability generated by *Family IV* will destabilize the swarms much longer at slow inclination than at higher inclination. Moreover, different waves of instability associated to the k -subfamilies of *Family IV* corresponding to $R_{I^*}^k$, cross successively the swarms, which may strengthen the inclination dependence. As shows Fig.3, the resonant rectangles can also overlap, ensuring the coexistence of at least two k -subfamilies in the same swarm. These intersection of rectangles and the associated dynamics are studied in the next section. In order to verify these predictions and to illustrate the geometry of the resonances of *Family IV*, we have integrated the L_4 Trojans swarm for several initial values of Saturn's semi-major axis a_2 . The associated configurations of the planetary system are represented in Fig. 3 by vertical lines, and the initial values of a_2 can be found in Tab. 2. The initial inclination of the Trojans are equal to 2° for the solid lines, labeled with small roman letter, and to 20° for

⁵ Strictly speaking, the function f is not smooth on an interval, but, according to the KAM theory, at most on a Cantor subset of this interval. But here, as the planetary system under consideration is very regular in studied region, we can assume that f is invertible on the whole considered interval.

the broken lines labeled with a capital letter. The present configuration of the solar system, widely studied in Paper I, is not discussed here, but is represented in Fig.3 by the vertical bold line located at $a_2 \approx 9.5855 AU$. As $\nu_{2,5}$ is close to $-1467 \text{ arcsec yr}^{-1}$, this implies that $-\nu_{2,5} \in 4\pi_g(\Theta_2)$ (light rectangle) and that $-\nu_{2,5} \in 5\pi_g(\Theta_{20})$ (dark rectangle), which is in perfect accordance with the results of Paper I.

3.2.2 Crossing of the Trojans swarms by the resonances of Family IV.

In this section, we will compare the previous predictions to numerical simulations of the L_4 swarm. In order to simplify the discussion, let us make an additional simplification. The integer j is already fixed to 1, and from now on, we do not take into account the secular frequencies s and s_2 . This omission is fully justified for small inclinations, and we will see later that even for an inclinations equal to 20° , the main resonances of *Family IV* are independent of s and s_2 . After the additional simplification, it is now more convenient to rewrite the relation (11) as:

$$g = -\frac{\nu_{2,5}}{k} + \frac{k-3}{k}g_1 + \frac{k'}{k}(g_2 - g_1) \quad (14)$$

This new formulation of a simplified *Family IV* enables us to exhibit some useful properties of these resonances.

(i) For a given value of a_2 , the right-hand side of (14) is a constant denoted g_r (for simplicity, the parameters k and k' are omitted).

(ii) Always for fixed a_2 : as long as k and k' are not too big, the relation $|\nu_{2,5}| \gg |(k-3)g_1 + k'(g_2 - g_1)|$ is satisfied (see Section 3.1.2). Therefore, the resonance is reached for value of g very close to $-\nu_{2,5}/k$. Consequently, we can see the *Family IV* as being split in different subfamilies parametrized by k . In every subfamily, a single resonance is defined by the additional parameter k' .

(iii) For a given k , the resonances of this subfamily are represented in the frequency space Θ_{I^*} by parallel planes which are separated by a distance of $(g_2 - g_1)/k$. Moreover, these planes are arranged in increasing order, in the sense that g_r increases with k' .

According to the property (ii), the resonant rectangles $R_{I^*}^k$ provide an approximation of the location of the k -subfamily which is valid as long as the combinations of the planetary secular frequencies involve in (14) are small with respect to $\nu_{2,5}/k$. Without going in too much details, we can consider that these boxes are minimal in the sense that: at least one of the resonances of the k -subfamily belongs to $R_{I^*}^k$, and that this resonance is always one whose dynamical influence is the largest. More precisely, except for $k = 3$, $g = -\nu_{2,5}/k$ does not satisfy the equation (14), and consequently does not correspond to any resonance of *Family IV*. But its closest resonant value, namely $-\nu_{2,5}/k + (k-3)g_1/k$, is reached for $k' = 0$ in formula (14). If this resonant value does not belong to the box $R_{I^*}^k$, one of the two frequencies $-\nu_{2,5}/k + (k-3)g_1/k \pm (g_2 - g_1)/k$ does. Moreover, the resonance associated to $k' = 0$, or one of its two closest neighbor, plays a central dynamical role in the subfamily

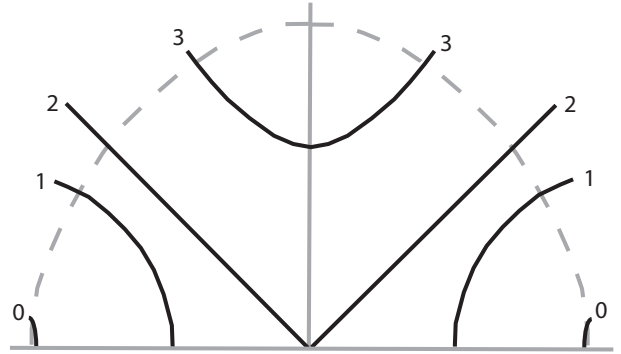


Figure 4. Schematic view of the displacement of a resonance of *Family IV* through the Trojans swarm. The X-axis represent the initial value of Trojan's semi-major axis. The initial eccentricity is associated to the Y-axis. The dashed curve approximates the limit of the stability region. The black curves correspond to the location of the same resonance for different values of Saturn's initial semi-major axis a_2 . The larger the label, the larger a_2 .

because its order is minimal. Here we use the classical definition of order, that is: $|k| + |k - k' - 3| + |k'|$. This integer quantity reaches a minimum of 3 for $k' = 0$, and it is generally assumed that the lower the order, the greater the resonance influence. Indeed, our method of localization neglecting the term $(k-3)g_1 + k'(g_2 - g_1)$ in equation (14). As $|(k-3)g_1| < 10 \text{ arcsec yr}^{-1} \ll g$ our method provides the value of a_2 for which the element of *Family IV* with $k' = 0$ belongs to $R_{I^*}^k$. Thus we predict when the strongest instability enters the Trojans swarm.

Figs 5 and 6 show respectively the sweeping of the Trojan region at $I^* = 2^\circ$ and $I^* = 20^\circ$ by the resonances of *Family IV*. Except for the values of I^* , the two figures are the same. The right bloc shows dynamical maps of the domains D_{I^*} , while the left one shows the projection of $\Theta_{I^*} = F(D_{I^*})$ on the plane of coordinates (g, s) .

As mentioned in section 3.1.1, we use the relative change of the frequencies, $\sigma_\nu = (\nu^1 - \nu^2)/\nu^1$, namely diffusion index, as an indicator of the regularity of the motion for a particular trajectory. In this formula, ν^1 is the libration frequency computed on the first 5 My, while ν^2 , is calculated on the following 5 My. In Figs. 5 and 6 (right bloc) we show several global pictures of the diffusion indicator, where we assign a color to $\log \sigma_\nu$. The color scale goes from blue, that corresponds to stable regions ($\sigma_\nu < 10^{-6}$), to red for very chaotic regions ($\sigma_\nu > 10^{-2}$). In black, we display the particles that have been ejected from the Trojans swarms during the integration (10 My).

It is important to mention that, as it is explained in Paper I, the phase space of Jupiter's Trojans is symmetric. More precisely, we can clearly observe two different type of symmetries. The first one, which was already visible in Michtchenko et al. (2001); Nesvorný & Dones (2002), is a symmetry with respect to a curve that is close to the straight line $a = a_1^{(0)} \approx 5.2035 AU$ (i.e., the initial semi-major axis of Jupiter), and tangent to it at L_4 . The second symmetry that we observe is the one with respect to a curve close to the axis $e = e_1^{(0)} \approx 0.0489$. Moreover, considering quasiperiodic trajectories, the fundamental frequencies corresponding to a given initial condition and the ones corresponding to one of its two symmetric points are the same. These frequencies

parametrize the KAM torus on which the given trajectories lie. This does not mean that the two corresponding trajectories are the same, but that they lie on the same invariant torus. From the dynamical point of view, these trajectories are equivalent. These symmetries point out the fact that there are manifolds (even close to L_4) where the frequency map is degenerated (see Gabern et al. (2005)). These symmetries allow us to restrict the sample of initial conditions to the subset $\{(a, e); a \geq a_1^{(0)}, e \geq e_1^{(0)}\}$.

In order to further clarify the relationship between the frequency space and the action space, let us add following comments. Figure 5.a (left) is made up of a union of curves (more or less smooth) that are the image of the lines $e_0 = \text{constant}$ by the Frequency Map F (it is also true for the other frequency maps, but owing the strong chaos, this is less obvious). The triangular shape of the picture is explained in the following way: the upper vertex of the triangle corresponds to the L_4 point, and the right and left edges correspond, respectively, to the line $e = 0.05$ (eccentricities lower limit) and to $a = 5.2035$ AU (semi-major axis lower bound). These curves are smooth in regular regions, but singularities arise in chaotic zones. Singularities of the Frequency Map are directly correlated with instabilities of the corresponding trajectories (see Laskar (1999) for more details). Along these curves ($e_0 = \text{constant}$), when a increases g increases too while the secular frequency s is decreasing. As a result, if we increase g keeping s constant, a increases while e becomes smaller. A striking example is given by the secular resonance $s = s_2$ marked by the read arc bounding the long time stability region in Fig.5.a-right. It is also represented in Fig.4 by the grey dashed curve.

Before going further, we will describe schematically the motion of a single resonance of *Family IV* during its crossing of the co-orbital region. Fig. 4 represent a section of the corresponding phase space in the plane (a, e) where the other initial elliptic elements are fixed. The horizontal straight line is the a -axis where $e = e_1^{(0)}$ while the vertical grey line is the e -axis where $a = a_1^{(0)}$. The two symmetrical sides of the phase space section are represented here ($a > a_1$ and $a < a_1$). The dashed grey curve gives the lower bounds of the strongly unstable region (black zone in Figs 5 and 6 right blocs). Let us assume that we start the evolution of the planetary system with an initial value of a_2 locating Saturn between Jupiter and the 5:2 MMR, in such a way that a_2 increases during the migration. As the planetary system get closer to the 5:2, the frequency $-\nu_{2,5}/k$ decreases toward zero ($\nu_{2,5}$ is negative in this region). Consequently the resonant frequency g_r , associated to the k -subfamily decreases too, and the first contact between the Trojans and this resonance arises at the two black segments labeled with 0, where a reaches its lower and greater value. Then, g_r keeping on decreasing (a_2 sill growing), the resonant goes centreward (black curve 1) to reach L_4 (label 2). Here, the two separated branches merge together to give the single curve (2). After the resonance travel through the vicinity of L_4 , it moves toward higher eccentricities (label 3) and leave the Trojans swarm crossing the secular resonance $s = s_2$ (at least for low to moderate initial inclinations).

In the light of the above discussion, the interpretation of Figs 5 and 6 is now easy. These figures are composed of two blocs. The right bloc corresponds to dynamical maps of the domain D_{2° (Fig 5) and D_{20° (Fig 6). The left bloc is the

Table 2. Resonances of *Family IV* represented in Figs 5 and 6. The two first columns indicates the label of the corresponding panel and the initial value of a_2 used for the associated numerical simulation. The two last columns gives the values of the integer k and k' defining by formula (14) the resonances represented by vertical lines on each panel of Figs 5 and 6.

Label	a_2 (AU)	k	k'
a	9.58986	4	$-1, \dots, 3$
-	-	3	$-2, \dots, 4$
b	9.59364	4	2, 3
-	-	3	$-2, \dots, 4$
c	9.59513	3	$-2, \dots, 4$
-	9.59513	2	-5
A	9.59630	4	2, 3
-	9.59630	3	$-3, \dots, 2$
d	9.59684	3	$-2, \dots, 4$
-	-	2	$-5, \dots, -2$
B	9.59756	3	$-3, \dots, 3$
C	9.597816	3	$-3, \dots, 3$
D	9.59882	3	$-3, \dots, 3$
e	9.60004	2	$-5, \dots, 2$
f	9.60057	2	$-5, \dots, 3$
E	9.60088	2	$-6, \dots, -2$
F	9.60197	2	$-5, \dots, 0$

corresponding view in the frequency space. The frequency map \mathcal{F} establishes the correspondence between these two blocs which are dynamically equivalent. Each bloc is made up of six panels, labeled from 'a' to 'f' at $I = 2^\circ$ and 'A' to 'F' at $I = 20^\circ$, associated to different values of $a_2^{(0)}$. These values are represented in Fig. 3 by vertical lines crossing the grey boxes. These values are chosen such that from 'a' to 'f' (resp. 'A' to 'F') Saturn's semi-major axis increases, letting the k -subfamilies of *Family IV* crossing the Trojans swarms following the rules established in section 3.2.1.

Resonances of *Family IV* are clearly visible in the frequency maps (left blocs), corresponding to vertical structures mad up of gaps or of accumulation of dots. These are enhanced by vertical dashed lines for $k' \neq 0$ and solid lines for $k' = 0$, where k' is the integer which occurs in formula (14) as the parameter of the k -subfamily. On the action side (right blocs), these resonances are less easy to identify. Although having the typical shape drawn in Fig.4, confusions are always possible with the elements of *Family II* that have also a quite similar form. The main resonances of *Family IV*, the ones which are drawn in Figs 5 and 6, are gathered together in Tab. 2. One find in its second column the initial values of Saturn's semi-major axis. The corresponding labels are in the first column. The two last columns correspond to the values of the integers k and k' occurring in formula (14) and which define the resonances of *Family IV* associated to the 2:5 MMR.

The secular resonance $s = s_2$ is also well identifiable in the left bloc by an horizontal line corresponding to an accumulations of dots at $s = -26$ arcsec yr $^{-1}$ surrounded by gaps. It has the property to split the frequency space in two different regions: the above part which is globally regular, assuming that the planetary system is not too close to the 5:2 MMR (it is true at least between the present Saturn's location $a_2 = 9.5855 \dots AU$ and 9.595 AU simulation c), and the part lying below this resonance which is strongly chaotic. This secular resonance (right bloc) appears in the actions

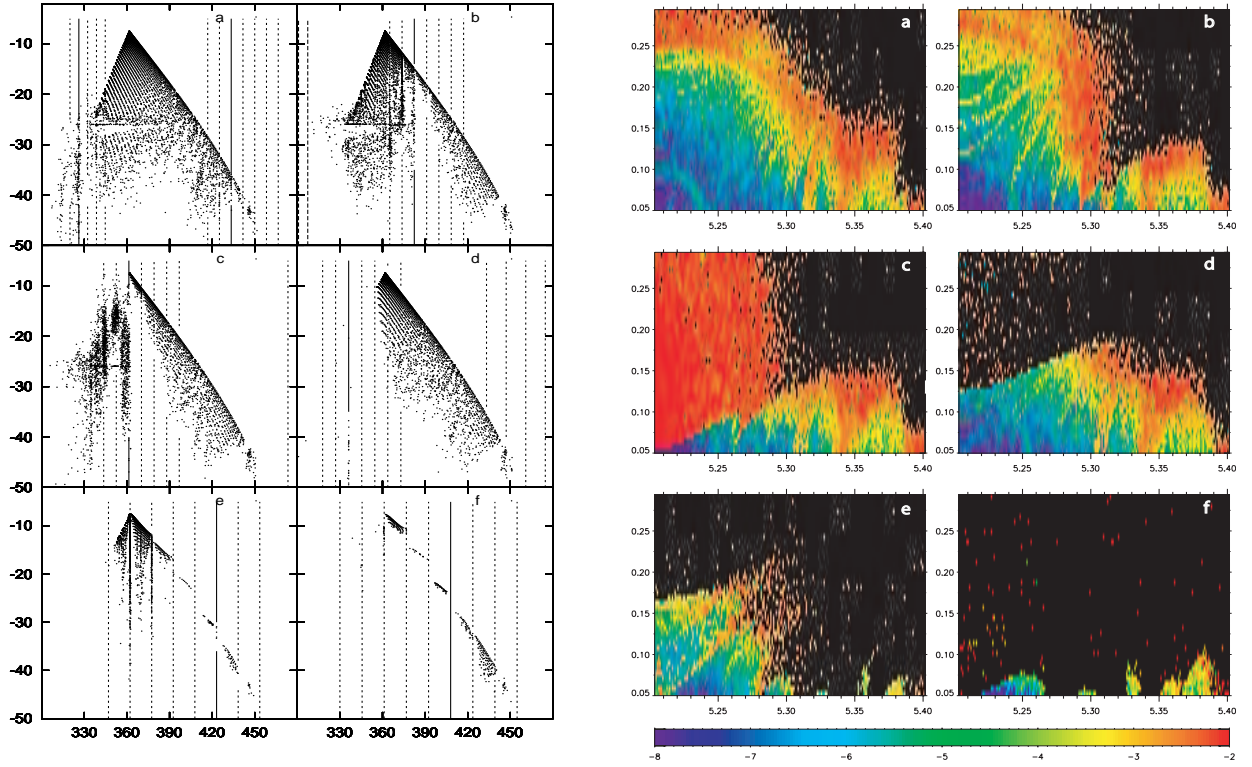


Figure 5. Destabilization of the Trojans swarms by the resonances of *Family IV* for $I^* = 2^\circ$. Left block: Dynamical maps in the frequency space (projection on the (g, s) plane). The vertical lines show the predicted location of the resonances of *Family IV* involved in the dynamical process (see Table 2). Right block: Dynamical maps in the action space (the initial conditions of the fictitious Trojans are chosen in the plane (a, e) , the four other elliptic elements being fixed). The diffusion rate defined by $\log_{10} \left| \frac{\nu^{(1)} - \nu^{(2)}}{\nu^{(1)}} \right|$ is coded by colors that vary from -8 (stable) to -2 (strongly chaotic). Each block is split in six panels labeled from "a" to "f" corresponding to the numerical simulations described in section 3.2.2. See the text for more details.

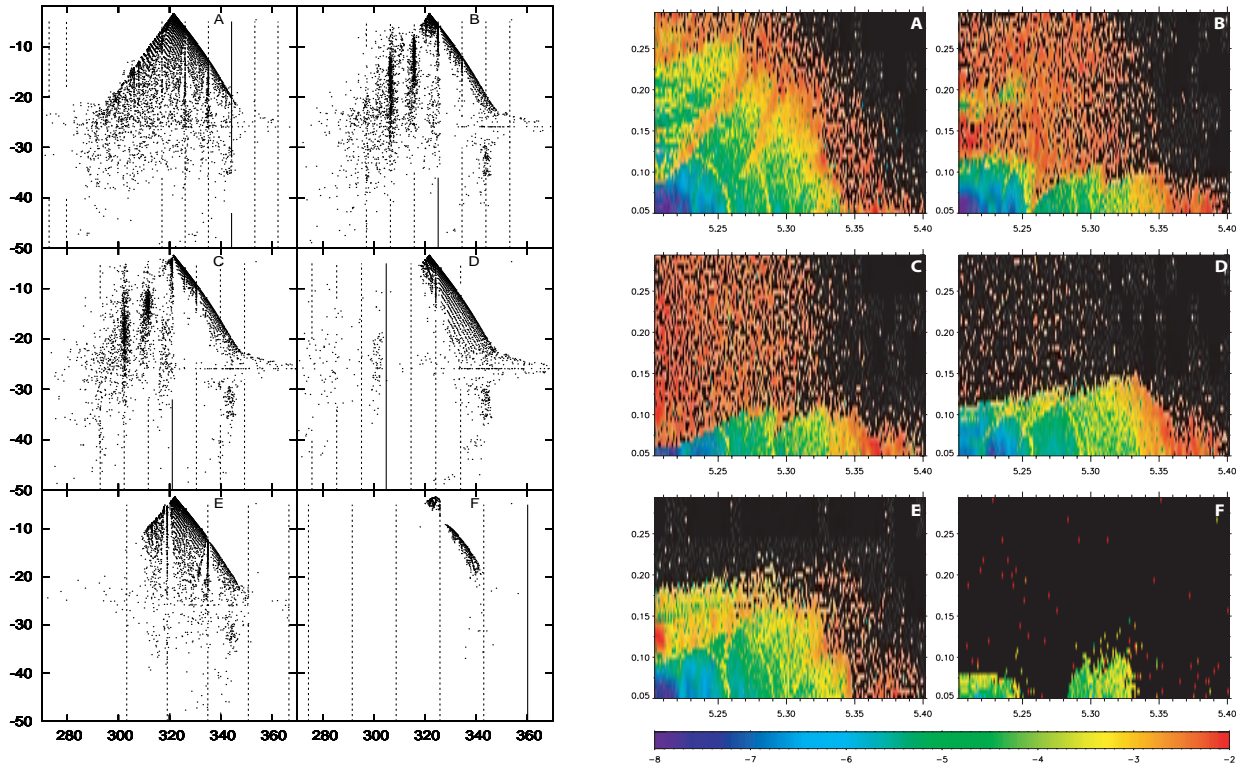


Figure 6. Same as Fig. 5 for $I^* = 20^\circ$.

space as the red arch that cuts the vertical axis at about $e = 0.25$ and the horizontal one at $a = 5.35AU$. As mentioned above, Fig. 5.a reveals that the domain located inside this arch (blue to green color) is much more regular than the outside part (orange to black). For small eccentricities, $s = s_2$ overlaps with the *Family I* resonance defined by formula (7) with $i = 1$ et $j = 13$ red V-shape, generating this large chaotic region around $5.34AU$. *Family I* is also acting around $5.4AU$ where the narrow red strip corresponds to $i = 1$ et $j = 14$. But, as in this experiment, the semi-major axis of Saturn varies only very few, about one hundredth of AU (see Tab. 2), only the resonances of *Family IV* move, while those belonging to the three other families are practically fixed. This makes easier the recognizing of the resonances of *Family IV*.

According to Paper I, the present system (vertical bold line in Fig. 3) is such that the 4-subfamily of *Family IV* is acting on low inclined Trojans. For slightly larger a_2 both 4-subfamily and 3-subfamily are involved in the Trojans dynamics. In Fig.5.a, the 4-subfamily is exiting the phase space (the corresponding resonances are located around $g = 330$ arcsec yr^{-1}), while the 3-subfamily penetrates inside. For $k = 4$, the subfamily mainly appears above $s = s_2$ at high eccentricities ($e > 0.25$), and strengthens the instability induced by the secular resonance. The 3-subfamily appears at the opposite side of the frequency space and are very difficult to identify in the action space because they are located in a region already filled by the resonances of *Family I* mentioned above (read V-shape surrounding $a_2 = 5.35AU$). It is worth mentioning that the narrow gap at $a = 5.38AU$ in Fig. 5.a is generating by the *Family IV* resonance defined by $k = 3$ and $k' = 1$. This resonance will play a major role in the next experiment. When a_2 is slightly larger, simulation 'b' ($a_2 = 9.59364AU$), the situation is much more interesting. Indeed, the subfamily $k = 3$ begins to reach central regions, generating strong instability associated to a rapid escape of numerous Trojans, particularly for $a > 5.31AU$. Another important point lies on the fact that this subfamily encounters elements of *Family II*. This overlap generates the deep gap located at $5.31AU$. The involved *Family II* resonances are defined by the multiplet $(\alpha, \beta, i, j, k, l, l_s) = (1, 2, 5, 2, 0, 0, 0)$ in formula(10) and are identifiable in Fig. 5.a by the quite vertical orange structure between 5.31 and $5.32AU$ (Its location is practically unchanged in Fig. 5.a). Regarding the involved resonance of the 3-subfamily, it is defined by $k' = 1$, and its neighbor ($k' = 0$) is also visible on the left of the previous one, marked by the small red V-shaped structure. For eccentricities higher than 0.075 these two resonances overlap too, contributing to this large ejection zone neighboring the above mentioned gap.

In panel 'c', the 3-subfamily continue to cross the Trojans swarm, and now occupies its core. The resonance associated to $k' = 0$ is now very close to L_4 (curve 2 in Fig 4) while previous ones ($k' < 0$) are on the other side of L_4 (curve 3 in Fig 4). The overlap of these resonances (for $k' \neq 0$) generates the huge red region above the resonance $k' = 0$, while the other part of the phase space begins to be a bit more regular. In panel 'd', the 3-subfamily moves outward but its resonances are still acting for $e > 0.13$. The sharp transition between the black region and the blue one is due to the resonance defined by $k = 3$ and $k' = 2$. below

this resonance, the size of the stable region (blue to green) is increasing again. Remarks that the effect of the 2-subfamily (right side of the frequency map) is not yet noticeable. Finally, when the 2-subfamily penetrates deep inside the Trojans swarm, the situation becomes more tragic. In panel 'e', a huge number of Trojans escapes the co-orbital region in less than ten million years, while in 'f', only small islands of temporary stability remains. The comparison between 'f'-left and 'f'-right shows that each island is separated by two consecutive resonances of the 2-subfamily. This is possible because the distance between two resonances of the previous kind is larger than the one separating the resonances of the 3 and 4-subfamilies. The simulation 'f' is the last one of the sequence. Indeed, if Saturn get closer to the 5:2 MMR, the entire Trojans Swarm is rapidly cleared. At $9.602AU$, (see Fig. 3), the frequency $-\nu_{2,5}$ decrease abruptly to reach the MMR. During this decrease, the 1-subfamily is reached, but at the same time, the planetary system crosses the 'separatrix' of the 5:2 MMR. The chaos induced by the separatrix crossing combined with the resonances of *Family IV* make the whole Trojans Swarm strongly unstable. We will see in section 3.3 that this phenomenon stops when the planetary system is inside the stable domain of the libration area associated to the 5:2 MMR.

At 20° of initial inclination, the mechanism is practically the same, but a bit delayed. Indeed, in simulation 'c' ($I^* = 2^\circ$) and 'C' ($I^* = 20^\circ$) the dynamical situation is basically the same, but 'c' occurs at $a_2 = 9.59513AU$ and 'C' at 9.597816 . This is a direct consequence of the fact that the upper bound of $\pi_g(\Theta_{I^*})$ is a decreasing function of I^* . This would have implications on the final distribution of the Trojans versus inclination, as we will see in the end of the present section. Looking at Fig. 6 (left bloc), one realizes that the main chaotic structures are vertically aligned. This confirms the choice, which could seem arbitrary, that we have made in formula (14). Indeed, resonances of *Family IV* which generates the most chaotic behavior do not depend on s, s_j . Conversely, these secular nodal frequencies are involved in secular resonances. In addition to the resonance $s = s_2$, which is still visible at 20 deg, two other resonances can be seen in Fig. 6 (right bloc). These structures form the two yellow thin arches (particularly in 'A') cutting the X-axis at $5.26AU$ for the $3s - s_2 - 2g_1 = 0$ (inner arch), and $5.29AU$ for the $2s - 3g_1 + g_6 = 0$ (outer arch). As in Fig. 5, simulations 'A' to 'F' show the shifting of the resonances of *Family IV*. In 'A', the 4-subfamily is exiting the phase space while the 3-subfamily has already reached its center. The two resonances in both sides of L_4 are defined by $k = 3$ and $k' = -3, -2$. They are associated to the two quasi-straight lines, displayed in yellow-orange colors, crossing the two above-mentioned resonant arches. In 'B', the resonances are shifted leftward (frequency space) and their overlap generates global chaos above $e = 0.12$ (location of the resonance $k = 3, k' = -1$). Then, the resonance $k' = 0$ reaches L_4 and generates the sharp transition between blue and red regions. The 3-family moving outward, the stable area begins to shrink drastically between simulations 'D' to 'E'. In 'E', the 2-subfamily penetrates the phase space and eject the most of the Trojans in 'F'. As in simulations performed with an initial inclination of 2° , only small islands of temporary stability remain and are surrounded by gaps generated by the resonances of the 2-subfamily. The increas-

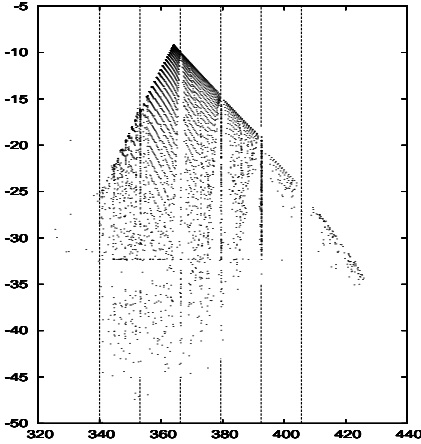


Figure 7. The 3:7 MMR and its *Family IV*: Θ_2 projected on the (g, s) plan for $a_2 = 9.1833AU$. From right to left the six vertical lines correspond to the resonances $2g = -\nu_{3,7} - 2g_1 + k'(g_2 - g_1)$ for $-k \in \{1, 2, 3, 4, 5, 6\}$. The frequency unit is the arcsec yr^{-1} .

ing of the stable region between crossing of two subfamilies of *Family IV* is something that we have not observe at low inclinations for a simple reason.

As it was already mentioned, the length of the interval $\pi_g(\Theta_{I^*})$ decreases with the increasing of I^* . The main consequence, which is illustrated in Fig. 3, is that the size of the boxes associated to a given subfamily decrease when the inclination get higher. Consequently, the higher the inclination, the less possible the intersection of two boxes. Indeed The clear boxes intersect and not the dark ones. As a result, between two successive subfamilies, renewal of stability may occur for high enough values of I^* . This phenomenon can be also seen in Fig. 8 second panel, where the fraction of ejected Trojans decreases suddenly from 0.8 to less than 0.6 to finally jump to 0.9 and more (see section 3.3 for more details).

To complete this section, let us point out that the above-mentioned evolution may lead to a lack of weekly inclined bodies Trojan. Indeed, if we assumed that the migration stopped close enough to the MMR, the sweeping of the Trojans would have taken place for small inclinations while it wouldn't have begun for higher inclinations. Unfortunately, in the solar system, Jupiter and Saturn are too far from the 5:2 MMR to have generated this phenomenon; except if this system was closer, in the past, to the resonance than it is now. But it seems not to be a realistic scenario.

3.2.3 Family IV associated to other orbital resonances

The mechanism studied in section 3.2.2 being very general, resonances of *Family IV* should take place in a small neighborhood of each MMR. But in some cases, the corresponding region is so chaotic that no resonance can be accurately identified. This is particularly true for the 2:1 orbital resonance, where its merging with *Family II* generates a huge unstable zone (see section 3.3).

On the other hand, the resonances of *Family IV* associated to the 7:3 MMR can be easily detected, essentially because they generate a moderate chaos. We consider here that the initial semi-major axis of Saturn is equal

Table 3. Secular resonances: values of a_2 (in AU) for which the three first resonances of the form $g = g_2 + k(g_2 - g_1)$ enter the intervals Θ_2 , Θ_{20} , and Θ_{30} for the "elliptic section" ($M_2 = 340.04^\circ$).

I^*	$g = g_2$	$g = 2g_2 - g_1$	$g = 3g_2 - 2g_1$
2°	< 8.39	[8.41, 8.425]	[8.43, 8.455]
20°	< 8.395	[8.425, 8.43]	[8.45, 8.46]
30°	< 8.4	[8.435, 8.44]	[8.47, 8.475]

to $a_2 = 9.1833AU$. Fig. 7 displays the projection of the Trojans frequency domain Θ_2 on the plan of coordinates (g, s) . For this planetary configuration, which is very close to the 7:3 MMR, the combination of proper mean motion $\nu_{3,7} = 3n_1 - 7n_2$ is close to $-423 \text{ arcsec yr}^{-1}$, implying the relation $-\nu_{3,7}/2 \in \pi_g(\Theta_2)$. Consequently, several resonances of the 2-subfamily, defined by the relation:

$$2g = -\nu_{3,7} - 2g_1 + k'(g_2 - g_1), \quad (15)$$

are present in the Trojans phase space. Fig. 7 shows those resonances for $k' \in \{-6, -5, -4, -3, -2, -1\}$. Let us notice that the horizontal line, corresponding to the secular resonance $s = s_2$, is shifted downward in comparison with Fig. 5. Indeed, s_2 was equal to about $-26 \text{ arcsec yr}^{-1}$ in the simulations of section 3.2.2 while here, its value is close to $-32 \text{ arcsec yr}^{-1}$.

3.3 Role of the secondary resonances

The main purpose of this section is to find out, in the most exhaustive possible way, which are the unstable structures being able to affect Trojans swarms during a migration phase. As mentioned in section 3.1.1, we limit our study to the domain $a_2 \in [8, 9.65]AU$, which locates Saturn between the 2:1 and the 5:2 MMRs. This goal can be reach by, at least, two different ways. The first one consists on the prediction of these events knowing, on one hand the behavior of the planetary frequencies, on the other hand the four families of resonances generating chaotic behaviors. The second way rests on numerical simulations of the same kind than the ones presented in section 3.2.2 and 3.2.3.

We have followed independently these two different paths and have found results in very good agreement. These results are presented in Fig 8. Among the numerous data produced by these numerical simulations, we only plot the ejection rate, that is: the number of escaping Trojans divided by the amount of bodies present in the initial population.

Fig. 8 is split in four panels. The bottom frame (8.d) shows the predicted location of the resonances generating instabilities, it will be detailed latter on. The three other panels display the depletion rate (Y-axis) with respect to the initial semi-major axis of Saturn (X-axis, in AU). They correspond to simulations with initial inclination equal to $I^* = 2^\circ$ in Fig.8.c, $I^* = 20^\circ$ (8.b), and $I^* = 30^\circ$ (8.a). On these depletion curves, the succession of steep peaks of ejection (local maximum of ejection) and deep troughs of stability (local minimum of ejection) provide useful indications on the global dynamical behavior of the Trojans swarms along the migration path.

Before going further, let us notice that, in the present Solar System, Jovian Trojans are located in a trough of

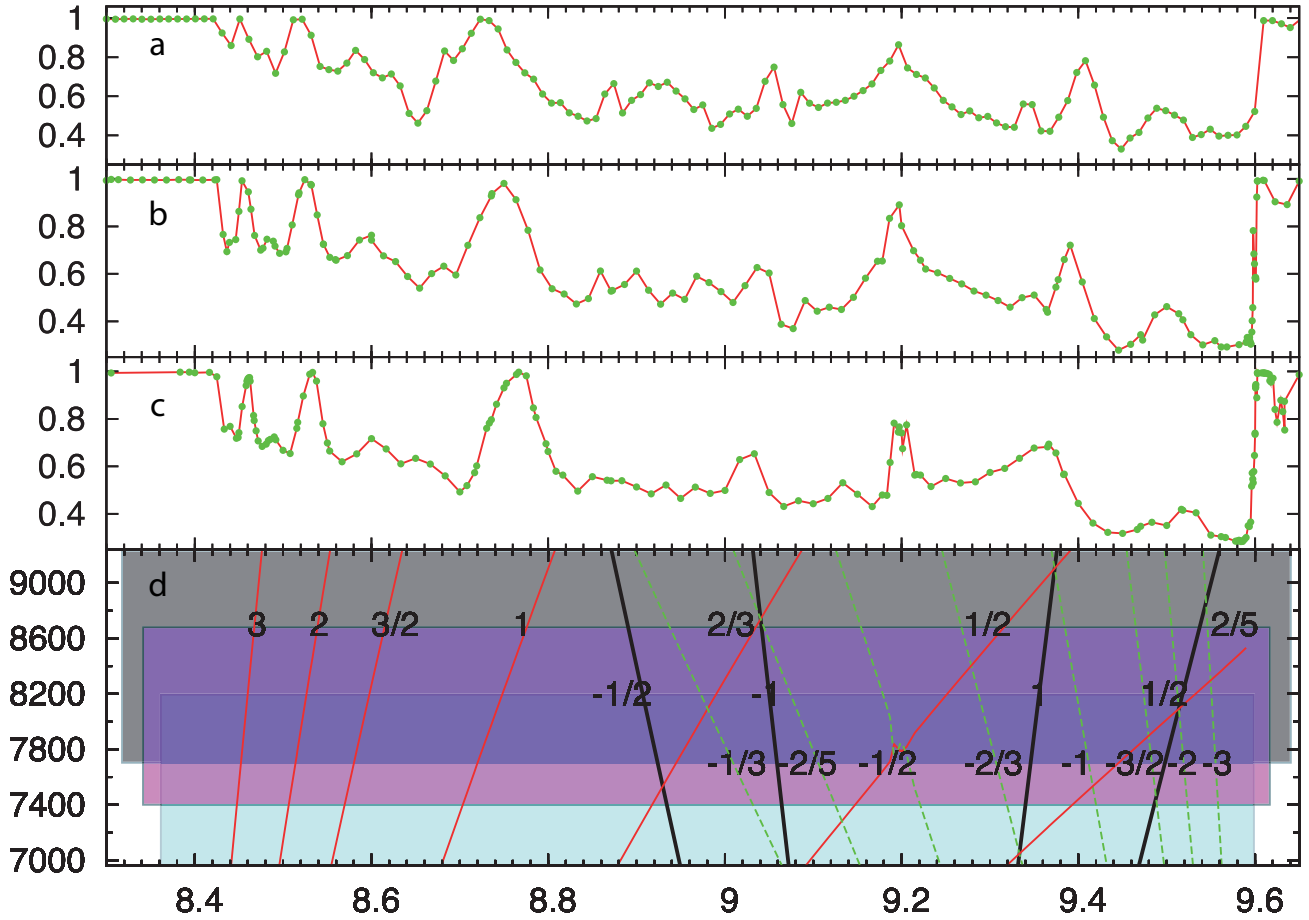


Figure 8. Chaos generated by the resonances of *Family II*: on the bottom frame (d), the frequencies $\nu_{1,2}, \nu_{3,7}, \nu_{2,5}$ and some of their rational multiples are plotted versus a_2 . The rational numbers written on the curves $i/j\nu_{(\alpha,\beta)}$ correspond to the value of i/j , the values of (α, β) being equal to $(1, 2)$ for the red curves, $(3, 7)$ for the black bold ones and $(2, 5)$ for the green dashed curves. The horizontal grey, pink and blue strips indicate the reachable values of ν in Θ_2 , Θ_{20} , and Θ_{30} . The three upper plots represent the relative number of ejected trojans n_{eject} (escape rate) during our numerical integration (section 3.1.1) of respectively \mathcal{D}_{2° (panel c), \mathcal{D}_{20° (b) and \mathcal{D}_{30° (a) for $a_2 \in [8.3, 9.65]$ AU.

strong stability ($a_2 = 9.5855 \text{ AU}$). It may be amazing that the migration would stop where the stability of the Trojans swarms were maximal. But in fact, other planetary configurations leading to stable swarms exist. In particular, $a_2 = 9.44 \text{ AU}$ provide a nice solution to this problem. Fig. 8 shows that this solution is perhaps the most stable that we have explored, particularly at 20° and 30° of initial inclination.

The ejection peaks present in Fig. 8 are obviously associated to resonances. The following reasoning will show that, except three peaks, the other ones are generated by resonances of *Family II*. Let us first consider these three particular cases. Those unstable regions are indirectly generated by the three main MMRs present in the studied domain: the 2:1 for $a_2 < 8.4 \text{ AU}$ (in fact this is more a plateau than a peak, in this whole region the depletion rate is about 100%), the 7:3 at $a_2 = 9.2 \text{ AU}$ and the 5:2 for a_2 around 9.6 AU and more. As mentioned in section 3.1.2, the both sides of these peaks are generated by action of *Family IV* conjugated to the chaos introduced by the planets crossing the separatrix of the MMRs. When the planetary system is deep inside the 7:3 and mainly 5:2 MMRs, the depletion rate decrease suddenly, which suggest the existence

of regions harboring stable Trojans. This is especially striking at $I^* = 2^\circ$. This phenomenon has been pointed out in Marzari & Scholl (2007) where authors find long live Trojans when Jupiter and Saturn are in the 2:1 orbital resonance. We do not observe the same stability in this resonance as we can see in Fig. 8 where the ejection rate is always close to 100%. These different behaviors can be explained quite easily. Indeed, Trojans stability depends strongly on the location of the planetary system with respect to the different topological structures of the considered MMR. If the planets inside the resonance are close a separatrix (hyperbolic manifold) of one of these structures, the chaos induced by the planets may destabilize the whole Trojans swarm. On the contrary, if the planets lie in a stable region corresponding for example to an elliptic libration centre, their motion is in general close to quasiperiodic. Consequently, the Trojans do not suffer from chaos induced by the planetary system. But the motion of the Trojans is not necessarily regular. Secondary resonances between ν and the libration frequency associated to the MMR can arise, leading the ejection of numerous Trojans. Without studying the MMRs one by one, we cannot know which case corresponds to a given situation. We can only mention that, around 9.63 AU , where a

region of relative stability takes place inside the 5:2, the angle $2\lambda_1 - 5\lambda_2 + 3\varpi_2$ is librating, and according to Fig. 2, our 'elliptic migration path' crosses some kind of libration center (one of the most stable regions encountered in the section of the phase space). On the contrary, when Jupiter and Saturn are in 2:1 MMR ($a_2 \leq 8.4AU$), almost all Trojans are ejected from the co-orbital zone. This is probably because our migration path stays always quit far from the libration center of the 2:1 orbital resonance (see Fig. 2).

Concerning the other ejection peaks, they are certainly not associated to *Family I*. The reason is that, this family depends mainly on n_1 which varies only very few in our simulations. Consequently, resonances of *Family I* have rather the same strength all along the migration path and thus cannot be responsible of these successive stability changes.

The same argument holds for the secular resonances of *Family III*. The secular resonance most affecting Jovian Trojans is the $s = s_2$. It moves continuously (except in a small neighborhood of the MMRs) without coming close to L_4 . Other higher order secular resonances including nodal secular frequencies can eventually move inside the Trojans phase space, but generate only a very local chaos (see section 3.2.2). A very interesting point is connected to the existence of the secular resonances $g = (k + 1)g_1 - kg_2$, which can play an important role in increasing the eccentricity of the Trojans belonging to. Basing on the values of g_1 and g_2 given in Fig. 1 and according to formulas (12), the exact location of these resonances can be derived. Tab. 3 gives the locations of the main resonances of this kind. According to Fig. 8 these values correspond to a region which is close to the 2:1 MMR, and where very high peaks are present. We will go back to this point latter, but in any case, the influence of secular resonances seems to be very local and cannot generate this succession of highly unstable regions.

Having eliminated the other resonances, only *Family II* remains. It is not, in fact very amazing because of at least two reasons. The first one is that we have shown in section 2.3 that these resonances were able to act far away from their associated MMR. Furthermore, Paper I reports that, in the present solar system, narrow unstable regions resulting from *Family II* appear in Θ_{I^*} . The second reason lie on the fact that in Morbidelli et al. (2005), the authors point out two strong instabilities which enable the capture of the future Jupiter Trojans.

In order to make sure that these peaks are really due to *Family II*, we will compare, like in section 3.2.2, our predictions to the simulations whose results are plotted in Fig. 8. To predict the locations of Saturn whose resonances of *Family II* penetrate the Trojans swarms, we proceed as for *Family IV*: neglecting the right-hand side of the equality (10), that is, the combination of secular frequencies, the resonance condition writes: $\nu = \frac{2}{7}\nu_{\alpha,\beta}$. The question is now to know whether, for a given a_2 , the frequency $\frac{2}{7}\nu_{\alpha,\beta}$ belongs to $\pi_\nu(\Theta_{I^*})$ or not. The bottom frame of Fig. 8 answers the question: for the three main MMRs, namely $(\alpha, \beta) \in \{(1, 2), (3, 7), (2, 5)\}$, the values $\frac{2}{7}\nu_{\alpha,\beta}$ are plotted versus a_2 . The X-axis represents a_2 in AU while the vertical axis measures the frequencies in arcsec yr^{-1} . A color is associated to each MMR, the curves $\frac{2}{7}\nu_{\alpha,\beta}$ (which are practically straight lines) are drawn in red for the *Family II* connected to the 2:1 MMR, in black for the one associated to the 7:3 and in green for the 5:2. The black labels on

these lines indicate the values of $\frac{2}{7}$ associated to the corresponding resonance. For the sake of clarity, these labels are aligned. The upper line (located at about 8600 arcsec yr^{-1}) corresponds to $\nu_{1,2}$, the second line (at 8200) to $\nu_{3,7}$, and the last one (at 7600) to $\nu_{2,5}$. The colors of the background correspond to the values of the initial inclination I^* . The grey is associated to $I^* = 2^\circ$: more precisely, in the grey region, the frequencies (Y-axis) range in the interval $\pi_\nu(\Theta_{2^\circ})$. In the same way, in the pink rectangle, the frequencies belong to $\pi_\nu(\Theta_{20^\circ})$, and to $\pi_\nu(\Theta_{30^\circ})$ for the cyan domain. The use of these different colors allows predicting easily the location of resonances for the three inclinations used in this paper.

As it was the case for *Family IV*, the criterion $\frac{2}{7} \in \pi_\nu(\Theta_{I^*})$ does not correspond to a single resonance in the Trojans phase space but rather to multiplet of resonances associated to the linear combination of secular frequencies arising in the right hand side of (10). Consequently narrow strips should replace the lines. But for the sake of simplicity, we prefer to keep the lines.

In Fig.8.a-c, between the 2:1 MMR (left) and 8.8 AU, three high peaks stand out for all inclinations (the ejection rate is practically equal to 100%). As it was mentioned above, the resonances of *Family II* associated to the 2:1 MMR dominate this region; therefore, these three strong depletion zones are generated by these resonances. Indeed, these peaks coincide perfectly with the lines labeled with 3, 2 and 1 (bottom frame) associated to the relations: ν equal 3, 2 and 1 times $\nu_{1,2}$. These maximum of ejection match very well the prediction: the bases of the peaks coincide with the projection on the X-axis of the intersection of the corresponding line with the colored region (e.i. pink for $I^* = 2^\circ$). More over, the peaks are shifted rightward when the inclination grows, which is due to the fact that red lines are increasing. We have to mention that it is not the first time that these structures are observed. Indeed, in Morbidelli et al. (2005), the authors have widely studied the region corresponding more or less to the interval [8.3, 8.65] AU in our simulations (see next section). They found two regions of strong depletion corresponding to our two first peaks. Moreover, in Fig. 1 of the above-mentioned paper, the curve indicating the fraction of population that survives for $2 \cdot 10^5$ My in the co-orbital region possess a small singularity (just after 1.5 My of integration) which is not mentioned in the paper. Looking at Fig. 8, we clearly see that this singularity is generated by the subfamily $\nu = \frac{3}{2}\nu_{1,2}$.

Our main peak, corresponding to the encounter of the secondary resonance $\nu = \nu_{1,2}$ is outside of the region studied in Morbidelli et al. (2005), but it seems that an important phenomenon occurs here. Indeed, the rightward shift of this structure when I^* increases is very important compared to the two previous peaks. It is essentially because the slope of the red curved representing the frequency $\nu = \nu_{1,2}$ is smaller than the ones of the curves $\nu = 2\nu_{1,2}$ and $\nu = 3\nu_{1,2}$. F. Marzari and H. Scholl (2007) mention the existence of this resonance but observe that it is weaker as compared to the previous secondary resonances (the 1:2 and 1:3). It is not what we get in our study, but the two simulations are not easy to compare. The first simulation takes into account a forced migration, imposing Trojans to cross a given resonance quite rapidly. While in our case, the migration being frozen, the resonances have enough time (here 10 My) to eject the test-particles. In any case, we probably over-

estimate the influence of the resonances, but our goal is not to have a realistic simulation of Jupiter’s Trojans during the planetary migration, but to point out the regions or the events that are relevant in term of eject (or injection) of bodies in the co-orbital region. In the same paper F. Marzari and A. Scholl stress the dominant role of the secular resonance $g = g_2$. In our simulation, the region where $g = g_2$ occurs is so close to the 2:1 MMR (see Table 3) and so chaotic that the fundamental frequencies are meaningless: Trojan’s trajectories are too far from quasiperiodic ones. But, in the contrary, for $I^* = 2^\circ$, we can distinguish a very small peak centered at $a_2 = 8.44AU$ (just before the secular resonance $\nu = 3\nu_{1,2}$) which is generated by the secular resonance $g = 3g_2 - 2g_1$. By increasing I^* , the secular resonance is shifted rightward (Table 3) while the secondary goes leftward. This generates an overlap at approximately 20° (commune peak in Fig.8.b). This 2 regions are split again for higher inclination (Fig.8.a). Nevertheless the dynamical influence of the resonance $\nu = 3\nu_{1,2}$ seems to be always predominant.

When the semi-major axis of Saturn is greater than $8.8AU$, the dynamical situation becomes richer but more complicated. Indeed, the resonances of *Family II* generated by the frequency $\nu_{1,2}$ are still present, but although they are involved in the global dynamics of the present solar system (see Paper I), their dynamical influence decreases strongly. On the other hand, the secondary resonances of *Family II* associated to $\nu_{3,7}$ and above all $\nu_{2,5}$ begin to generate instabilities.

On one hand, the order of the 2:5 and 3:7 MMR being greater than the one of the 1:2, the corresponding resonances of *Family II* will probably less perturb the Trojans swarms than the ones depending on the 2:1. On the other hand, one can expect to find strong chaos when at least two of these resonances overlap. Let us notice that, because $\nu_{3,7} = \nu_{1,2} + \nu_{2,5}$, when a resonance of *Family II* associated to $\nu_{1,2}$ and another one associated to $\nu_{2,5}$ overlap (intersection of red lines and green lines in Fig.8.d) a secondary resonance connected to $\nu_{3,7}$ is present in the same place. But generally, the order of this resonance is quite high. As we have retained only the resonances $\nu = \pm\nu_{3,7}$ and $2\nu = \pm\nu_{3,7}$ (the resonances associated to $\nu = \pm 2\nu_{3,7}$ are also of interest, but for the sake of clarity they are not drawn in the figure) only four triple intersections are inside the studied domain (Fig. 8.d). These intersections are defined by the relations:

$$\nu = \frac{2}{3}\nu_{1,2} = -\frac{2}{5}\nu_{2,5} = -\nu_{3,7} \quad \text{at about} \quad 9.04AU \quad (16)$$

$$\nu = \frac{2}{5}\nu_{1,2} = -\frac{2}{3}\nu_{2,5} = \nu_{3,7} \quad \text{at about} \quad 9.33AU \quad (17)$$

$$\nu = \frac{1}{2}\nu_{1,2} = -\nu_{2,5} = \nu_{3,7} \quad \text{at about} \quad 9.37AU \quad (18)$$

$$\nu = \frac{2}{5}\nu_{1,2} = -2\nu_{2,5} = \frac{1}{2}\nu_{3,7} \quad \text{at about} \quad 9.5AU \quad (19)$$

These four different overlaps coincide with a local maximum of the ejection rate. The most striking phenomenon occurs when the resonances of the *Family II* associated to $\nu = \nu_{3,7}$ cross the Trojans space phase, see formulas (17) and (18), for $a_2 \in [9.33, 9.37]AU$. Indeed, at $I^* = 30^\circ$ (Fig.8.a), rises a steep peak reaching 80% centered at $9.41AU$, while a smaller one is located on its left at $9.3AU$. When the initial inclina-

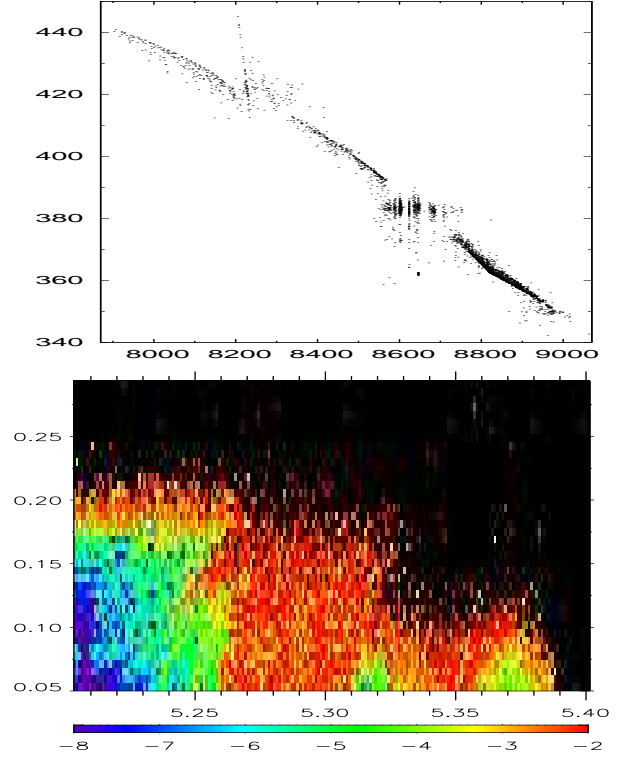


Figure 9. Overlap of resonances of *Family II* associated to 2:5 MMRs. Top frame: projection on the frequency plane (ν, g) where the resonances are easy to identify (see the text for more details about this resonances). Bottom frame: chaos generated by these resonances in the plane (a, e) .

tion falls from 30° to 2° , these two unstable structures merge to generate the rounded peak around $9.37AU$ (Fig.8.c). The predictions given in Fig.8.d suggest that the left above mentioned structure is generated at 30° by the triple resonance defined by the equation (17), while the right one by the intersection of the $2\nu = \nu_{1,2}$ and the $\nu = -\nu_{2,5}$ secondary resonances. When I^* decreases, the higher pick follows the *Family II* resonances associated to $\nu = -\nu_{2,5}$ and is consequently shifted leftward, while the other one is driven by the $\nu = \nu_{1,2}$ and goes rightward. The merging of those two structures occurs at $I^* = 2^\circ$ (Fig. 8.c) generating the high rounded peak generated by the intersection defined by the relations (18). The last resonance maintained the relatively high level of ejection on the left side of the peak.

In order to illustrate this discussion, the L_4 Trojans swarm has been integrated in the case of $a_2 = 9.3842AU$ and $I^* = 2^\circ$. As a_2 is slightly greater than the location of the triple resonance defined by (18), and according to (Fig. 8.d), the resonance of *Family II* generated by $\nu = -\nu_{2,5}$ should dominate the global dynamics of the swarm. This is exactly what reveals the top panel of Fig.9. This figure shows the projection of Θ_{2° on the plane (ν, g) . Details concerning this projection can be found in Paper I. Two structures are particularly interesting: the resonance overlap (accumulation of vertical segments) around $\nu = 8600 \text{ arcsec yr}^{-1}$ and the slant line at about $8200 \text{ arcsec yr}^{-1}$. The first structure to the overlap of the resonances of *Family II* of the kind: $\nu = -\nu_{2,5} - kg_1 + (k-3)g_2$, where $k = -1, 0, 1$ have been clearly identified. This overlap leads to the wide red region

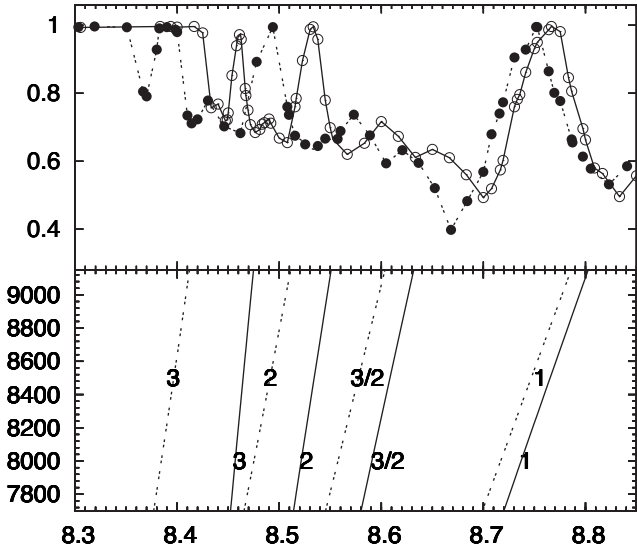


Figure 10. Initial phases dependence of the resonances of *Family II*: the bottom frame shows the predicted locations of the resonances $\nu \approx 3\nu_{1,2}$, $\nu \approx 2\nu_{1,2}$, $\nu \approx 3/2\nu_{1,2}$ and $\nu \approx \nu_{1,2}$ (see Fig. 8-d), for the "elliptic section" in solid lines and for the "hyperbolic section" in dashed lines. The top-frame shows the ejection rate for these two sections.

lying between $a_2 = 5.25$ and $5.31AU$ in the bottom panel of Fig.9. As regard the secondary structure, it is generated by the resonance $\nu = -\nu_{2,5} - g - 2g_2$ which is probably the main generator of the second chaotic structure corresponding to the red area surrounding $a_2 = 3.35AU$ in the bottom frame of Fig. 9.

We will not give further comments concerning Fig.9, but the bottom frame of this picture allows the reader to understand by himself the existence and the inclination dependence of the smaller ejection peaks present in Fig.9.

3.4 Initial phases dependance

Adiabatic invariance theory suggests that, during the migration, the planets are never captured in MMRs (Morbidelli et al. 2005). For this reason, and even if we do not take migration into account, we will study the evolution of the resonant structure along the "hyperbolic segment" defined in section 3.1.2. Contrarily to the "elliptic segment", the previous one has the advantage to cross the 2:1 resonance at its smallest section, minimizing the range of Saturn's semi-major axis for which the two planets are trapped inside the MMR. This simulation is probably closer than what is expected by adding planetary migration.

Denoting by $\nu_{1,2}^H$ the quantity $n_1 - 2n_2$ evaluated along the hyperbolic segment (Fig.1 green curve) and $\nu_{1,2}^E$ the one computed on the elliptic path (Fig.1 red curve), we deduce from Fig.1 that when $a_2 \in [8.3, 8.85]$ and is out side of the MMR, the inequality $\nu_{1,2}^E < \nu_{1,2}^H$ holds. Moreover, the greater a_2 , the smaller the the value of $\nu_{1,2}^H - \nu_{1,2}^E$. In addition, the width (in a_2) of the 2:1 MMR along the two sections are very different: the "elliptic width" is about three times greater than the hyperbolic one (see also Fig. 2). As a result, the slop of the red curve is always greater than the slope of the green one. These facts have direct consequences

on the secondary resonances of *Family II* associated to $\nu_{1,2}$. Fig.10 details the comparison between these two choices of initial phases. In its bottom frame, the frequencies 3, 2, 3/2 and 1 times $\nu_{1,2}$ are represented in solid lines for $\nu_{1,2}^E$ and in dashed lines for $\nu_{1,2}^H$. Just like Fig1-d, this plot enables us to predict the location of the resonances of *Family II*. The associated numerical simulations are reported in the top frame of Fig.10⁶, the ejection rate of the hyperbolic section are represented by a dashed curve with black circles while the solid line with white circles is used for elliptic section. One more time, the numerical simulations and the predictions are in very good agreement. As regards the location of the resonances of *Family II*, a given resonance is crossed by the Trojans swarm at a smaller value of a_2 in the hyperbolic case than in the elliptic one, the splitting between these two locations decreasing when the planetary system moves away from the orbital resonance. The width of the resonances of *Family II* is also affected by the change of the initial phases of the planetary phases. Because the slop of the curves plotted in the bottom frame of Fig. 10 is smaller for the elliptic section than for the hyperbolic section, the resonances generated in the hyperbolic case are wider than the ones associated to the elliptic case. But, as shown in Fig. 10, even if the ejection peaks are wider and shifted leftward along the hyperbolic section, the global features are the same in the both cases. Consequently, we think that the modification of the planetary phases does not really affect the global dynamics of the Trojans swarms.

4 DISCUSSION

We have shown that the global dynamics of a Trojans swarm is shaped by its resonant structure. This structure depends crucially on the fundamental frequencies of the planetary system in which it is embedded. We have established the link between the modifications of the geometry of the planetary system and the change of stability of the Trojans swarm. In order to study the global dynamics of Trojan in a system whose planets migrate, it is enough to know the evolution of the fundamental frequencies of the system during its migration. Therefore, without even integrating the particles of the swarm, we can determine the main features of its global dynamical evolution (transition between total stability and strong instability). In our application to the case of Jupiter Trojans disturbed by Saturn, we have varied one parameter: the semi-major axis of Saturn⁷. In a realistic migration, many other parameters would vary, but we think that this modifies only slightly the results obtained in this paper. Indeed, we have seen in section 3.4 that the variations of the planetary phases almost did not affect our results. In the same way, the "apsidal corotation" of the planetary perihelia which, according to Marzari & Scholl (2007), strengthen the influence of the secular resonances, probably does not significantly modify the resonant structure of the Trojans.

⁶ In this section, the simulations are limited to the Trojans having an initial inclination equal to 2° , which is enough for the study of the phases dependence.

⁷ If we had varied the semi-major axis of the two planets, it would have been easy to keep a one parameter model by using, rather the two semi-major axis of the planets, their ratio.

Another interesting point can be deduced from our study. The resonant structure, and particularly its splitting in four families defined in section 2.3 are generic. Moreover, the definition of the families seems to hold for almost all planetary configurations. But the respective dynamical influence of the four families depends on the mass of the planet harboring the Trojans swarms. According to (1), if this mass decreases, the decrease of the proper frequency g is proportional to the planetary mass while the one of ν is weaker ($\nu = O(\sqrt{\varepsilon})$). The elements of *Family IV* being approximated by the relation: $g \approx \nu_{p,q}$, the smaller the planetary mass, the closer this resonance from the $p : q$ MMR. As a result, the smaller the mass of the planet, the more local the dynamical influence of *Family IV*. In this case, we can expect that the role of the resonances of *Family IV* becomes negligible compared the one played by *Family II*. Conversely, the secular resonances (*Family III*) which do not involve the frequency s , seem to be negligible in the Jovian Trojans swarm. But, their contributions increase for smaller planetary mass, as it was already mentioned in section 2.3.

Finally, the method of prediction developed in this paper being very general, this approach can be used to study the dynamics of a large class of problems. Beside its straightforward application the Trojans of a planet (results concerning the dynamics of the hypothetical Trojans of Saturn will be presented in a forthcoming paper), it can also be used to study the dynamics of satellites in a planetary system in migration, or more generally, to understand the behavior of a dynamical system undergoing quasiperiodic perturbations with slowly varying frequencies.

Acknowledgments

This work has been partially supported by PNP-CNRS. The computing clusters IBM-SP4 at CINES have been widely used.

References

- Benettin G., Fasso F., Guzzo M., 1998, *Regul. Chaotic Dyn.*, 3, 56
- Brasser R., Lehto H. J., 2002, *MNRAS*, 334, 241
- Celletti A., Giorgilli A., 1991, *Celest. Mech. Dyn. Astron.*, 50, 31
- Danby J. M. A., 1964, *Astron. Astrophys.*, 69, 165
- Deprit A., Deprit-Bartholome A., 1967, *Astron. J.*, 72, 173
- Deprit A., Henrard J., Rom A., 1967, *Icarus*, 6, 381
- Efthymiopoulos C., Sándor Z., 2005, *MNRAS*, 364, 253
- Érdi B., Nagy I., Sándor Z., Süli Á., Fröhlich G., 2007, *MNRAS*, 381, 33
- Gabern F., 2003, PhD thesis, Departament de Matemàtica Aplicada i Anàlisi Universitat de Barcelona
- Gabern F., Jorba À., 2004, *Astron. Astrophys.*, 420, 751
- Gabern F., Jorba A., Locatelli U., 2005, *Nonlinearity*, 18, 1705
- Garfinkel B., 1976, *Celestial Mechanics*, 13, 229
- Gascheau G., 1843, *Compt. Rend.*, 16, 393
- Giorgilli A., Delshams A., Fontich E., Galgani L., Simó C., 1989, *J. Differential Equations*, 77, 167
- Giorgilli A., Skokos C., 1997, *Astron. Astrophys.*, 317, 254
- Gomes R. S., Morbidelli A., Levison H. F., 2004, *Icarus*, 170, 492
- Holman M. J., Wisdom J., 1993, *Astron. J.*, 105, 1987
- Jorba À., 2000, *Astron. Astrophys.*, 364, 327
- Jorba A., Simó C., 1996, *SIAM J. Math. Anal.*
- Laskar J., 1990, *Icarus*, 88, 266
- Laskar J., 1999, in Simó C., ed., *NATO ASI, Hamiltonian Systems with Three or More Degrees of Freedom*. Kluwer, Dordrecht, pp 134–150
- Laskar J., Robutel P., 2001, *Celest. Mech. Dyn. Astron.*, 80, 39
- Laskar J., Robutel P., Joutel F., Gastineau M., Correia A. C. M., Levrard B., 2004, *Astron. Astrophys.*, 428, 261
- Leontovitch A., 1962, *Dolk. Akad. Nouk USSR*, 43, 525
- Levison H., Shoemaker E., Shoemaker C., 1997, *Nature*, 385, 42
- Lhotka C., Efthymiopoulos C., Dvorak R., 2008, *MNRAS*, 384, 1165
- Markeev A. P., 1972, *Soviet Astronomy*, 15, 682
- Marzari F., Scholl H., 2007, *MNRAS*, 380, 479
- Marzari F., Tricarico P., Scholl H., 2003, *MNRAS*, 345, 1091
- Meyer K. R., Schmidt D., 1998, *J. Differential Equations*, 62, 222
- Meyer K. R., Schmidt D., 2005, *J. Differential Equations*, 214, 256
- Michel P., 1997, *Astron. Astrophys.*, 328, L5
- Michtchenko T., Beaugé C., Roig F., 2001, *Astron. J.*, 122, 3485
- Milani A., 1993, *Celest. Mech. Dyn. Astron.*, 57, 59
- Milani A., 1994, in *IAU Symp. 160: Asteroids, Comets, Meteors 1993 Vol. 160, The dynamics of the Trojan asteroids*. pp 159–174
- Morais M. H. M., 2001, *Astron. Astrophys.*, 369, 677
- Morais M. H. M., Morbidelli A., 2002, *Icarus*, 160, 1
- Morais M. H. M., Morbidelli A., 2006, *Icarus*, 185, 29
- Morbidelli A., Levison H. F., Tsiganis K., Gomes R. S., 2005, *Nature*, 435, 462
- Murray C. D., Dermott S. F., 1999, *Solar System Dynamics*. Cambridge univ. press
- Nekhoroshev N. N., 1977, *Russian Math. Surveys*, 32, 1
- Nesvorný D., Dones L., 2002, *Icarus*, 160, 271
- Rabe E., 1967, *Astron. J.*, 72, 9
- Roberts G., 2002, *J. Differential Equations*, 182, 191
- Robutel P., Gabern F., 2006, *MNRAS*, 372, 1463
- Robutel P., Gabern F., Jorba A., 2005, *Celest. Mech. Dyn. Astron.*, 92, 53
- Robutel P., Laskar J., 2001, *Icarus*, 152, 4
- Scholl H., Marzari F., Tricarico P., 2005a, *Icarus*, 175, 397
- Scholl H., Marzari F., Tricarico P., 2005b, *Astron. J.*, 130, 2912
- Skokos C., Dokoumetzidis A., 2001, *Astron. Astrophys.*, 367, 729
- Tabachnik S. A., Evans N. W., 2000, *MNRAS*, 319, 63
- Tsiganis K., Gomes R. S., Morbidelli A., Levison H. F., 2005, *Nature*, 435, 459
- Yoder C., 1979, *Icarus*, 40, 341